Local ergodicity as a probe for chaos in quantum systems: Application to the Henon–Heiles system

B. Ramachandran and Kenneth G. Kay
Department of Chemistry, Kansas State University, Manhattan, Kansas 66506

(Received 26 August 1986; accepted 12 January 1987)

Classical chaos is usually accompanied by "local" ergodicity—ergodic behavior in regions of phase space that are generally smaller than, but of the same dimensionality as, the energy surface. If there are strong bottlenecks in phase space impeding the relaxation to statistical equilibrium in the full region of ergodicity, it is often possible to define an approximate form of ergodic behavior in a smaller subregion where relaxation occurs temporarily but quickly. Such "pseudoergodicity" is also a symptom of chaos. We use the presence of quantum behavior that mimics local ergodicity and pseudoergodicity as a probe for the influence of classical chaos on quantum dynamics. We show that the quantum analog of a pseudoergodic region in phase space is generally formed by superpositions of energy eigenstates. The superposition states spanning a given pseudoergodic zone have similar expectation values and small off-diagonal elements to other states with similar energy for a certain class of operators. We perform calculations which identify the ergodic regions for two versions of the quantum Henon–Heiles system. For the "more classical" of these systems we find good agreement between the proportion of quantum states in pseudoergodic zones and the proportion of classical phase space occupied by chaotic trajectories. We also find that the quantum pseudoergodic regions can be identified with classical vague tori of the precessing and librating types. Different ergodic regions are separated from one another by what appear to be the quantum analogs of the precessor–librator separatrix and other classical bottlenecks. For the "less classical" of the systems, we find that classical chaos is reflected in the quantum dynamics to a smaller, but still noticeable, degree.

I. INTRODUCTION

Classical systems that are nonintegrable typically undergo a transition from regular to irregular motion over a certain energy range.[1] The nature and the underlying causes of this transition have been the subjects of many studies.[1,2] In this paper, we investigate the implications of the transition and the resulting chaos for quantum mechanical systems. Our approach makes use of the intimate connection between the classical concepts of irregular motion and ergodicity.

To explain our approach, we must first establish some terminology. The dynamics of an s-dimensional system with smooth potentials is said to be regular if, for the vast majority of trajectories, the motion is confined to s-dimensional tori embedded in the $2s$-dimensional phase space. Such motion is stable, in the sense that the separation between initially nearby trajectories increases only linearly with time. Apart from rare cases of frequency commensurability, the motion on each torus is also ergodic on that torus,[1,3] i.e., any trajectory on a torus comes arbitrarily close to every point on the same torus during the course of time. We refer to this type of ergodicity as "trivial" because the ergodic region—the s-dimensional torus—has a lower dimensionality than the full $(2s-1)$-dimensional energy surface and thus has zero measure on the energy surface.

On the other hand, dynamics becomes irregular or chaotic when, for a substantial fraction of trajectories, the motion is no longer confined to tori, but extends over regions of higher dimensionality. Such motion is unstable, in the sense that neighboring trajectories diverge exponentially with time. Barring exceptional cases in which chaotic dynamics remains subject to certain supplementary integrals of motion,[4] the dimensionality of the chaotic regions is $(2s-1)$—the same as that of the energy surface. The chaotic motion may be said to be ergodic in these $(2s-1)$-dimensional regions since ergodicity in an invariant region is simply equivalent to the metrical indecomposability of that region.[5] An ergodic region of this kind still does not usually extend over the full energy surface.[1,2] However, it generally has nonzero measure on the energy surface since it has the same dimensionality as that surface. We therefore call the form of behavior usually accompanying chaos "nontrivial" ergodicity. For brevity, the term ergodicity will henceforth denote nontrivial ergodicity unless otherwise indicated.

Thus, chaotic behavior typically creates (nontrivial) ergodic regions in phase space. It may be conjectured that the converse is also true: the appearance of such ergodic regions in phase space signals the presence of chaos in Hamiltonian systems. Indeed, we are unaware of any cases where nontrivial ergodicity occurs in a Hamiltonian system (with $s>1$) without all of the accompanying manifestations of chaos, including exponentially diverging trajectories.

A traditional way of measuring the "degree of chaos" in a classical system is to calculate the fraction of the energy surface occupied by chaotic trajectories. For example, various authors have determined this degree by estimating the proportion of the Poincaré surface occupied by exponentially diverging trajectories,[6,7] by analyzing the distribution of frequency components in power spectra,[8] and by examining

 0021-9606/87/084628-20$02.10

the convergence of resummed perturbative expansions[9] at each energy. The present considerations show that this degree of chaos is directly related to the proportion of the energy surface occupied by ergodic regions.

In this paper, we identify the quantum counterparts of classical ergodic regions. We then extract information about the influence of chaos on quantum dynamics by comparing the "quantum ergodic" regions to those affected by classical chaos and by comparing the fraction of the quantum energy shell occupied by such regions to the classical degree of chaos. We thus use the concept of ergodicity to explore the consequences of chaos for quantum systems.

To establish criteria for identifying quantum counterparts of classical ergodic regions, we generalize the semiclassical ergodic theory which we previously developed.[10,11] In its earlier form, this theory applied only to "global" ergodicity on the full energy surface; for our present work we require a version that applies to "local" ergodicity on a limited portion of the energy surface. Criteria obtained from the resulting theory have the advantage of reducing to the classical criteria for ergodicity as $\hbar \to 0$. It is precisely this property that allows us to refer to the behavior observed in the quantum system as the counterpart of the classical behavior.

The implications of classical chaos for quantal systems has remained a controversial topic despite a large amount of work on this subject. There have been many attempts to identify the consequences of classical chaos for the energy levels,[12–14] wave functions,[15–18] matrix elements,[10,11,19–21] and dynamics[22–26] of quantal systems. There have also been previous attempts[13,14,25,27,28] to extract from such studies a quantum mechanically derived quantity that is analogous to the fraction of chaotic trajectories on the energy surface. Of the previous approaches to defining such a "quantum degree of chaos" the one that appears to be most successful relates this degree to the distribution of quantum energy level spacings.[13,14] As we shall see, the present approach effectively relates this degree to the dynamical behavior of the quantum system and to the distribution of certain quantum matrix elements.

Our work is certainly not the first attempt to use ergodicity as a means of identifying the implications of chaos for quantum systems.[10,11,15,20–22,29,30] However, the form of ergodic behavior investigated in earlier studies has been global ergodicity on the full energy shell—a condition not achieved by typical mechanical systems with smooth potentials. As we have emphasized, the form of ergodicity that actually accompanies the onset of chaos in such classical systems is local ergodicity. It appears that a proper treatment of the local nature of the ergodicity is crucial if one wishes to use ergodicity to relate classical chaos to quantum dynamics. For that reason, the present paper focuses on the local form of ergodicity as a key to exploring the influence of chaos on quantum mechanical behavior.

The remainder of this paper is based on the following plan: in Sec. II, we extend the definition of classical local ergodicity to quantum systems by applying the semiclassical ergodic theory. We thereby develop the theoretical concepts and techniques that allow us to identify locally ergodic regions in quantum systems. In Sec. III, we use these techniques to identify the ergodic regions in the quantum Henon–Heiles system. In Sec. IV, we compare the "quantum ergodic" regions and the "quantum degree of chaos" obtained from our calculations to the corresponding classical quantities and discuss the extent to which our results reflect various features of the underlying classical chaotic behavior. In Sec. V, we summarize our work and make concluding remarks.

II. THEORY

We begin by reviewing the classical definition of (local) ergodicity. Let us denote the Hamiltonian of a system by $H(\mathbf{p},\mathbf{q})$ and let $\rho(\mathbf{p},\mathbf{q})$ be the density function for a particular, invariant portion of the energy surface over which the ergodicity of the motion is to be examined. This function is the microcanonical density function $\delta[E - H(\mathbf{p},\mathbf{q})]$ multiplied by a characteristic function that is equal to 1 for points $(\mathbf{p},\mathbf{q})$ in the region of interest and 0 elsewhere. The invariance of the region implies that ρ does not evolve in time, i.e., $\rho[\mathbf{p}(t),\mathbf{q}(t)] = \rho[\mathbf{p}(0),\mathbf{q}(0)] = \rho(\mathbf{p},\mathbf{q})$, where $[\mathbf{p}(t),\mathbf{q}(t)]$ are the phase variables that evolve at time t from the variables $(\mathbf{p},\mathbf{q})$ at initial time 0. Then the motion in this region is said to be ergodic[1,3,5,31] if[10,11,32]

$$\lim_{T\to\infty} \overline{C}_A(T) = C_{A,\mathrm{eq}} \tag{1}$$

for all quadratically integrable dynamical properties $A(\mathbf{p},\mathbf{q})$, where

$$\overline{C}_A(T) = (1/T)\int_0^\infty dt \exp(-t/T) C_A(t), \tag{2}$$

$$C_A(t) = \langle A(t)|A\rangle / \langle A|A\rangle, \tag{3}$$

and

$$C_{A,\mathrm{eq}} = |\langle 1|A\rangle|^2 / \langle 1|1\rangle\langle A|A\rangle, \tag{4}$$

with

$$A = A(\mathbf{p},\mathbf{q}), \tag{5}$$

$$A(t) = A[\mathbf{p}(t),\mathbf{q}(t)], \tag{6}$$

and

$$\langle A|B\rangle = \int d\mathbf{p} \int d\mathbf{q}\, \rho(\mathbf{p},\mathbf{q}) A(\mathbf{p},\mathbf{q})^* B(\mathbf{p},\mathbf{q}). \tag{7}$$

In these equations, $C_A(t)$ is the autocorrelation function of property A, $\overline{C}_A(T)$ is the time average of this correlation function, and $C_{A,\mathrm{eq}}$ is the statistical equilibrium value of this function, where each of these quantities is evaluated over the region projected onto by $\rho(\mathbf{p},\mathbf{q})$. Equation (1) then states that the motion within this region is ergodic if the infinite time average of the autocorrelation function is equal to its statistical equilibrium value. The only difference between this definition of local ergodicity and the more familiar definition of global ergodicity is that, in the latter, the density function $\rho(\mathbf{p},\mathbf{q})$ which projects onto only a portion of the energy surface, is replaced by the microcanonical density function $\delta[E - H(\mathbf{p},\mathbf{q})]$ which projects onto the full surface.

The condition for ergodicity can be stated in a more concise form as[11]

$$\lim_{T\to\infty} F_A(T) = 0 \tag{8}$$

for all quadratically integrable A (except functions depending only on H), where

$$F_A(T) = [\overline{C}_A(T) - C_{A,\mathrm{eq}}]/(1 - C_{A,\mathrm{eq}}). \tag{9}$$

The quantity $F_A(T)$ was introduced in a previous study[11] which treated the special case $\rho(\mathbf{p},\mathbf{q}) = \delta(E - H)$. The conclusions derived there can be extended in a straightforward way to the present case to establish the following results: (a) $F_A(0) = 1$, (b) $F_A(T)$ is a monotonically nonincreasing function of T, (c) $F_A(T)$ obeys the inequality

$$0 \leqslant F_A(T) \leqslant 1 \tag{10}$$

for all T and (d) $F_A(T) = 1$ for all T when the dynamics in the region described by ρ is nonergodic and A [$\neq A(H)$] is any constant of the motion in that region.

The primary advantage of describing the condition for ergodicity in terms of the $F_A(T)$ instead of the $\overline{C}_A(T)$ and $C_{A,\mathrm{eq}}$ is that their normalization to the range between 0 and 1 allows us to identify behavior that is *close* to the ergodic ideal. As will become apparent below, this feature is important in establishing the quantum analog of ergodicity.

Thus, in terms of F_A, we may locate portions of the energy surface for which the dynamics is ergodic by searching for invariant regions of dimensionality $(2s - 1)$ for which $F_A(\infty) = 0$ for all quadratically integrable properties A. As discussed in the Introduction, such ergodic motion signals the presence of chaos.

One aspect of the procedure described above for identifying irregular regions of phase space is especially problematic for the proposed extensions to quantum systems. To verify the ergodicity of the dynamics, it is necessary to investigate the behavior of the system for periods of time that are at least long enough for the $\overline{C}_A(T)$ to relax sensibly to their equilibrium values. Often, however, such relaxation times are very long,[33–36] even for strongly chaotic systems, due to the temporary trapping of the phase flow by various "bottlenecks" within an ergodic region. The difficulty is that good agreement between quantum and classical dynamics often deteriorates after relatively short time periods[11,22,24] due to tunneling, nonclassical recurrences, and other quantal phenomena. Thus, if the relaxation of the $\overline{C}_A(T)$ is severely impeded by bottlenecks, serious differences between quantum and classical behavior may arise before the classical relaxation process is complete. Under such circumstances, it will not be possible to identify any form of quantum behavior that is similar to the ergodic behavior occurring in the classical system.[11] However, our main goal in the present studies is to identify the quantum analog of *chaotic* behavior and it is often possible to use the techniques of ergodic theory to detect chaos in classical systems even prior to the relaxation of the $\overline{C}_A(T)$ over the full ergodic region. It is these techniques that we extend to the quantum systems.

The techniques we require to identify chaos from the short-time behavior are applicable when the bottlenecks that divide an ergodic region into two or more parts are very strong. If the passage across such bottlenecks is slow enough, essentially complete relaxation may occur in each of the separated subregions long before relaxation occurs over the full ergodic region.[37,38] Under these circumstances, a form of "temporary ergodicity" applies to each of the subregions prior to diffusion across the bottlenecks, and the conditions specified by Eqs. (1) and (8) are fulfilled with the following changes: (a) the density function $\rho(\mathbf{p},\mathbf{q})$ appearing in the correlation functions is interpreted as the density function for one of the individual subregions; (b) $\overline{C}_A(\infty)$ and $F_A(\infty)$ are replaced by $\overline{C}_A(\tau)$ and $F_A(\tau)$, respectively, where τ is a time period that is shorter than the time required for a typical trajectory in the subregion of interest to escape across a bottleneck; (c) the functions $A(p,q)$ are restricted to those properties for which $\overline{C}_A(T)$ relax nearly completely by time τ; and (d) the equalities expressed in Eqs. (1) and (8) are replaced by near equalities. Thus, the content of Eq. (8), as presently modified, can be expressed as

$$F_A(\tau) \ll 1. \tag{11}$$

We call the temporary form of ergodicity described above "pseudoergodicity" to distinguish it from true ergodicity. Pseudoergodicity within a particular subregion is a reliable symptom of chaos provided that the subregion has dimensionality $(2s - 1)$.

In contrast to the condition for true ergodicity, the current condition for pseudoergodicity, Eq. (11), is not expressed in terms of a vanishing value of F_A. Since relaxation is generally incomplete during the finite observation time τ, $F_A(\tau)$ can, at best, be small but nonzero for all relevant properties A.

We note that the subregion projected by $\rho(\mathbf{p},\mathbf{q})$ is no longer truly invariant, as required by ergodic theory, since trajectories prepared in the subregion eventually "leak out" to the other portions of the full ergodic region. Nevertheless, under the assumed condition of separate time scales for relaxation within and among subregions, ρ is still approximately invariant up to time τ, i.e.,

$$\rho[\mathbf{p}(t),\mathbf{q}(t)] \approx \rho(\mathbf{p},\mathbf{q}), \quad t < \tau. \tag{12}$$

This approximate invariance is sufficient to allow us to extend most of the concepts associated with ergodicity to pseudoergodicity.

The kind of sequential relaxation needed for pseudoergodicity is expected to occur frequently. It is known, for example, that remnants of tori that have been partially destroyed by chaos can serve as bottlenecks to phase space flow.[37] Recent work by several groups[37,38] has identified cases in which the time scales for passage across such tori are so much longer than the relaxation rates within the separated subregions, that a form of transition state theory can be applied to calculate the rate of passage across the bottlenecks. Within the context of semiclassical mechanics, the regions to which chaotic trajectories are, at least temporarily, restricted have been called "vague tori."[9,39] The existence of these regions has been used to explain the success of certain semiclassical techniques to obtain quantized energy levels of chaotic systems.

We now use the principles of the semiclassical ergodic theory, as described in Refs. 10 and 11 to extend these ideas to quantum mechanics. This extension to quantum systems assumes that, apart from the total energy, the classically

chaotic behavior is not subject to any approximate, isolating, integrals of motion. Although the existence of exact, supplementary, integrals of motion for chaotic behavior is highly exceptional, the presence of approximate, supplementary, constants of motion is rather comnon in systems having more than two degrees of freedom.[40–42] When such approximate integrals restrict the classical motion to regions having dimensionality less than $2s-1$ for long periods of time, the treatment described below must be modified. These modifications are discussed in Appendix A.

Our objective here is to identify a quantum mechanical analog of $F_A(\tau)$ which can serve as an indicator of quantum behavior corresponding to classical chaos. Accordingly, we make the following substitutions in Eqs. (2)–(7) to obtain quantum analogs of the autocorrelation functions and their statistical equilibrium values: (a) we replace classical properties $A(\mathbf{p},\mathbf{q})$ and $A[\mathbf{p}(t),\mathbf{q}(t)]$ by $\hat{A}$ and $\hat{A}(t)$, where $\hat{A}$ is the operator corresponding to A and $\hat{A}(t)$ is $\hat{A}$ propagated for time t in the Heisenberg picture; (b) we replace the density function ρ by the projection operator $\hat{\rho}$ which projects onto those states on the quantum energy shell that correspond to the region described by the classical function; (c) we replace the phase space integrals by quantum mechanical traces. Thus, the quantum expressions for $C_A(t)$, $\overline{C}_A(T)$, and $C_{A,\mathrm{eq}}$ are given by Eqs. (2)–(4) with integrals $\langle A|B\rangle$ replaced by

$$\langle A|B\rangle^q = \mathrm{Tr}[\hat{\rho}\hat{A}^{\dagger}\hat{B}]. \tag{13}$$

We are now able to define the quantum analog of $F_A(T)$ in terms of the quantum correlation functions and equilibrium statistical values, obtained by the procedure described above. Using the superscript q to distinguish quantum analogs from the corresponding classical functions, we obtain

$$F_A^q(T) = [\overline{C}_A^q(T) - C_{A,\mathrm{eq}}^q]/(1 - C_{A,\mathrm{eq}}^q). \tag{14}$$

As in the classical case, it may be shown that $F_A^q(0)=1$ and that $F_A^q(T)$ is a nonincreasing function of T obeying the inequalities $0 \leqslant F_A^q(T) \leqslant 1$ for all T. The condition for quantum dynamics in the region projected by $\hat{\rho}$ to be considered analogous to classical ergodic or pseudoergodic behavior in the region projected by $\rho(\mathbf{p},\mathbf{q})$ is then

$$F_A^q(T) \simeq F_A(T) \quad \text{for} \quad 0 \leqslant T \leqslant \tau, \tag{15}$$

and

$$F_A^q(\tau) \ll 1 \tag{16}$$

for a class of operators $\hat{A}$ to be described below.

In order for the quantum and classical dynamics to be in good agreement for times τ, as required by these equations, it is necessary to choose quantities $\hat{A}$, τ, $\hat{\rho}$, and other parameters in a judicious way. As illustrated by the calculations of Ref. 11, a careful choice of these quantities can indeed cause the behavior of F_A^q to closely mimic that of F_A. We now discuss these optimal choices.

The set of operators $\hat{A}$ which is to be used to compute F_A^q and to test for ergodicity should, ideally, consist of all members of the class of "acceptable"[10] operators that are "not too strongly localized."[11] As discussed in Ref. 11, such operators correspond classically to well-defined quadratically integrable functions $A(\mathbf{p},\mathbf{q})$ that do not have exceptionally high values in regions of phase space of volume $\lesssim h^s$ and have many eigenstates on the quantum energy shell. Additionally, if we wish to test for pseudoergodicity instead of true ergodicity, the operators included in the calculations must correspond to classical properties that lead to nearly complete relaxation of the F_A by time τ. As in the classical case, properties $\hat{A}$ that are functions only of the Hamiltonian, $\hat{H}$, are not required to obey Eqs. (15) and (16).

Also as in the classical case, the observation time τ appearing in these equations must be long enough for the relaxation of the $\overline{C}_A^q(T)$ over the region of interest to be essentially complete, but short enough for the region to remain sensibly invariant. An additional requirement, dictated by the condition that F_A^q agree with F_A is that τ must be short enough for no serious discrepancies between quantum and classical dynamics to appear during this time period.

The density operators $\hat{\rho}$ appearing in the quantum autocorrelation functions are analogous to the functions $\rho(\mathbf{p},\mathbf{q})$ appearing in the classical autocorrelation functions. Thus, the $\hat{\rho}$ project onto locally ergodic or pseudoergodic portions of the quantum energy shell. To specify these operators, we recall the expression for the quantum analog $\rho^{\sigma}(E-\hat{H})$ of the microcanonical density function $\delta(E-H)$. This operator projects onto the full quantum energy shell and is used to define the quantum analog of global ergodicity. As discussed in Refs. 10 and 11, the microcanonical density operator is given by

$$\rho^{\sigma}(E-\hat{H}) = \sum_j |j\rangle \rho^{\sigma}(E-E_j)\langle j|, \tag{17}$$

where the $|j\rangle$ are energy eigenstates and the E_j are the corresponding energy eigenvalues. The quantity σ denotes the half-width of the quantum energy shell and $\rho^{\sigma}(E-E_j)$ is a function (e.g., a Gaussian) that decreases to zero as $|E-E_j|$ becomes much greater than σ. The value of σ must be chosen to contain enough energy levels that the dynamics occurring on the quantum energy shell closely mimic those occurring on the classical energy surface. More details about the choice of σ are given in Refs. 10 and 11.

The operator $\hat{\rho}$, needed to identify the quantum analog of local ergodicity, projects only onto the portion of the full energy shell associated with an ergodic region. Accordingly, we represent this operator as

$$\hat{\rho} = \sum_J{}' |J\rangle \rho^{\sigma}(E-E_J)\langle J|. \tag{18}$$

In this equation, $|J\rangle$ are states that span the ergodic or pseudoergodic region of interest and E_J are their energy expectation values. We do not require $|J\rangle$ to be energy eigenstates. Specific characteristics of the $|J\rangle$ are discussed at a later stage. The prime on the summation serves as a reminder that only certain states, corresponding to a particular ergodic region, are included. The function $\rho^{\sigma}(E-E_J)$ is defined as in Eq. (17), above.

The number of terms appearing in the restricted summation of Eq. (18) is determined, in part, by the requirement that the states projected by $\hat{\rho}$ represent regions of *nontrivial* ergodicity or pseudoergodicity, i.e., that the classical dimensionality of the regions be $2s-1$. We now discuss the relationship between the number of terms in Eq. (18) and

the dimensionality of the corresponding classical region.

Let us first express the classical distinction between trivial and nontrivial ergodicity as

$$\frac{\int d\mathbf{p}\int d\mathbf{q}\,\rho(\mathbf{p},\mathbf{q})}{\int d\mathbf{p}\int d\mathbf{q}\,\delta(E-H)}\begin{cases}=0 & \Rightarrow \quad \text{trivial ergodicity}\\ >0 & \Rightarrow \quad \text{nontrivial ergodicity,}\end{cases} \tag{19}$$

where the ratio on the left-hand side is simply the measure of the ergodic region projected by $\rho(\mathbf{p},\mathbf{q})$ with respect to the measure of the full energy surface. The quantum analog of this ratio is

$$\frac{\mathrm{Tr}[\hat{\rho}]}{\mathrm{Tr}[\rho^{\sigma}(E-\hat{H})]}=\frac{N_\rho}{N_E}, \tag{20}$$

where N_ρ is the number of states in the region projected by $\hat{\rho}$, while N_E is the number of states on the full energy shell. Applying the classical limit, we obtain:

$$\lim_{\hbar\to 0}\frac{N_\rho}{N_E}\begin{cases}=0 & \Rightarrow \quad \text{trivial ergodicity}\\ >0 & \Rightarrow \quad \text{nontrivial ergodicity.}\end{cases} \tag{21}$$

Although the number of states N_E on the energy shell is infinite in the classical limit, it is finite when $\hbar>0$. Equation (21) therefore leads us to expect N_ρ to vanish for a regular (trivially ergodic) region, away from the classical limit. This conclusion, however, has to be accepted with caution. Clearly, it cannot mean that there are never any quantum states on the energy shell that correspond to a classical torus since this would lead to absurd conclusions for a completely regular system where every state corresponds to a classical torus. Instead, the result $N_\rho=0$ does not apply to every torus but only to "almost every" torus. The condition then means that a classical torus selected at random from the energy surface will almost certainly not correspond to a quantum state. This is reasonable since only exceptional tori, obeying the EBK quantization conditions, can correspond to a quantum state, and such tori are of measure zero on the energy surface. Nevertheless, exceptional, quantized tori do exist and N_ρ will not be zero for a trivially ergodic region consisting of such a torus. The value we expect for N_ρ in this case is, in fact, just unity, consistent with the familiar rule that each quantized torus corresponds to a single quantum state. Thus, the quantum projection operator $\hat{\rho}$ for such a case should contain a single term of the form $|J\rangle\langle J|$. This expectation is supported by the explicit expression we derive for $F^q_A(\tau)$ [see Eq. (23), below]. This expression shows that, for a classically regular region, $F^q_A(\tau)$ cannot be close to zero for all acceptable properties as $\hbar\to 0$ unless $\hat{\rho}$ contains only a single term. If $\hat{\rho}$ contains more than one term, the resulting value of $F^q_A(\tau)$ will tend to 1 as $\hbar\to 0$ for quantum properties $\hat{A}$ that approach the true classical actions. Such a value for F^q_A contradicts the assertion of ergodic quantum behavior in the region.

Now let us turn our attention to the quantum counterpart of a classical region of nontrivial ergodicity. Since $N_\rho/N_E>0$ for such a region in the classical limit, we expect N_ρ also to be >0 for this region away from the classical limit. Actually, once again, we must be cautious. A classical region may correspond to a quantum state and N_ρ may be >0 only if its phase space volume $\int d\mathbf{p}\int d\mathbf{q}\,\rho(\mathbf{p},\mathbf{q})$ is at least on the order of h^s. However, even a classical nontrivial ergodic region that is large enough to yield the value $N_\rho=1$ is too small to be distinguished quantum mechanically from a trivially ergodic region, for which N_ρ may also be equal to 1. Only regions with $N_\rho>1$ may be confidently identified as counterparts of classical nontrivial ergodic regions. Thus, *in order to conclude that a quantum region is the analog of a nontrivially ergodic classical region*, i.e., that the corresponding classical region has dimensionality $(2s-1)$, *the density operator $\hat{\rho}$ in Eq.* (18) *must contain two or more terms.* Classical ergodic regions with $N_\rho=0$ or 1 are too small to yield quantum behavior that can be identified as chaotic.

We now discuss the choice of states $|J\rangle$ used to form $\hat{\rho}$, the projector onto an ergodic region. If, in analogy to the classical theory of true ergodicity, we insisted on the strict invariance of $\hat{\rho}$ for all times, then we would have to choose the $|J\rangle$ to be energy eigenstates. However, in analogy to the classical notion of pseudoergodicity, it is sufficient for our purposes to demand invariance of $\hat{\rho}$ for the limited time period τ, so that we may choose the $|J\rangle$ to be superpositions of energy eigenstates.

There are, actually two reasons for wishing to allow the $|J\rangle$ generally to be superpositions instead of individual energy eigenstates. First, it may be necessary to form linear combinations of energy eigenstates in order to create states that are localized in desired pseudoergodic subregions. Second, it may even be necessary to form such superpositions in order to create states that are localized in certain truly ergodic regions. A given energy eigenstate may be delocalized over several distinct ergodic subregions that are separated from one another by classical dynamical barriers. Although quantum transitions between these regions may be allowed by tunneling processes, the corresponding classical transitions may be forbidden. In such cases, density operators diagonal in the energy eigenstates project onto classical nonergodic regions and only operators diagonal in certain superpositions of these eigenstates can project onto individual ergodic zones.

If $\hat{\rho}$ is nondiagonal in the energy eigenstates, $\hat{\rho}$ will vary with time. To apply the tools of ergodic theory to such cases, this time dependence must be slow enough for the correlation functions to relax almost completely in the pseudoergodic or ergodic subregions prior to any significant breakdown in the invariance of $\hat{\rho}$. In Appendix B we examine the consequences of this requirement for the choice of states $|J\rangle$. We show there that the effective invariance of $\hat{\rho}$ over the time period $0\leqslant T\leqslant\tau$ implies that

$$\tau<\hbar/\Delta E, \tag{22}$$

where ΔE is the largest energy separation between the energy components of $|J\rangle$ and $\hbar/\Delta E$ may be interpreted as the invariance time of $\hat{\rho}$. The variety of superposition states $|J\rangle$ that may be used to represent pseudoergodic regions is thus constrained by restrictions that are placed on the invariance time. For example, the requirement that this time period greatly exceed the relaxation time of the correlation functions sets an upper limit to the separation between the energy components of the $|J\rangle$.

It is important to point out that the loss of invariance at

times $\approx \hbar/\Delta E$ may be caused by purely quantum effects (e.g., tunneling) as well as classical passage of trajectories across bottlenecks. Thus, although we refer to $\hbar/\Delta E$ as the invariance time, it may often be identical to what we call the time range for good quantum-classical correspondence.

In Appendix C we derive an explicit formula for $F_A^q(\tau)$. The result is

$$F_A^q(\tau) = B_A^{-1} \sum_J{}' \rho^\sigma(E - E_J)\,[\langle J|A|J\rangle - \langle A\rangle^q]^2 + B_A^{-1} \sum_J{}' \rho^\sigma(E - E_J) \times \sum_{\substack{K \\ K \neq J}} |\langle J|A|K\rangle|^2/[1 + (\omega_{JK}\tau)^2], \quad (23)$$

where

$$\langle A\rangle^q = \sum_L{}' \rho^\sigma(E - E_L)\langle L|A|L\rangle / \sum_L{}' \rho^\sigma(E - E_L), \quad (24)$$

$$B_A = D_A(1 - C^q_{A,\mathrm{eq}}), \quad (25)$$

$$\omega_{JK} = (E_J - E_K)/\hbar, \quad (26)$$

and the expressions for D_A and $C^q_{A,\mathrm{eq}}$ are given in Appendix C.

From Eq. (23), we see that the pseudoergodicity condition $F_A^q(\tau) \ll 1$ has the following implications for the matrix elements:

$\langle J|A|J\rangle$ = nearly constant for states $|J\rangle$ in a pseudoergodic region (27)

and

$\langle J|A|K\rangle$ = very small, for states $|J\rangle$ in a pseudoergodic region and states $|K\rangle$ of nearly equal energy. (28)

This result shows that the division of the classical energy surface into distinct chaotic regions implies a corresponding division of the quantum energy shell into sets of states having roughly constant expectation values for properties A and only small matrix elements of A to states of similar energy. The F_A^q simply provide numerical values that measure the dispersion in the expectation values and the average square of the off-diagonal matrix elements in the various regions. Equations (27) and (28) provide a generalization of conditions previously derived[10] for matrix elements of a quantum system whose classical counterpart is ergodic on the full energy shell.

An important question we have not yet addressed is how small $F_A^q(\tau)$ must be for the quantum dynamics to be considered analogous to the corresponding classical ergodic behavior. This is related to questions of how nearly constant $\langle J|A|J\rangle$ must be and how small $\langle J|A|K\rangle$ must be for states $|J\rangle$ in ergodic regions. To state this question in yet another way, we may express the "quantum ergodicity condition," Eq. (16), as

$$F_A^q(\tau) \leqslant \phi, \quad (29)$$

where $\phi \ll 1$ is a "cutoff" that distinguishes between values of F_A^q for ergodic and nonergodic regions, and inquire about the value for ϕ. Unfortunately, it is not possible to determine a universally valid, precise value of the cutoff. The difficulty is that, even in the case of *classical* ergodic or pseudoergodic dynamics, $F_A(\tau)$ depends on the observation time τ and, thus, the degree to which relaxation of the $\overline{C}_A$ is complete by the time quantum-classical differences appear or the pseudoergodic region breaks up. As a result, the condition for the quantum system to display behavior that is similar to classical ergodicity or pseudoergodicity, Eqs. (15) and (16), is necessarily somewhat imprecise. In part, this imprecision is an unavoidable consequence of applying the essentially classical concept of ergodicity to quantum systems. In Sec. IV we will discuss how the cutoff may be empirically determined under favorable circumstances.

Our final expression for F_A^q, Eq. (23), may be used to search the quantum energy shell for groups of states that exhibit dynamics analogous to classically chaotic behavior. This is accomplished by partitioning the energy shell into mutually exclusive regions, labeled by n, with corresponding density operators

$$\hat{\rho}_n = \sum_{\substack{\text{states in} \\ \text{region } n}}{}' |J\rangle \rho^\sigma(E - E_J)\langle J|, \quad (30)$$

where the $|J\rangle$ are either energy eigenstates or "almost stationary" superposition states obeying Eq. (22). For each region containing more than one such state, Eq. (23) is applied to compute $F_A^q(\tau)$ for various properties A. The behavior within a region is identified as pseudoergodic if these $F_A^q(\tau)$ are $\ll 1$ for all of the properties investigated. Finally, this process is repeated for additional partitions of the energy shell in an attempt to maximize the quantity

$$f_I(E) = \sum_n N_n/N_E, \quad (31)$$

where

$$N_n = \mathrm{Tr}[\hat{\rho}_n], \quad (32)$$

N_E is defined in Eq. (20), and the sum in Eq. (31) extends over the various pseudoergodic regions on the energy shell.

Maximization of f_I is appropriate here since participation of a quantum state in *any* nontrivial pseudoergodic or ergodic region indicates the influence of classical chaos on that state. Thus, we may not conclude that a quantum state is uninfluenced by chaos simply because it does not form part of an ergodic region for a *particular* partitioning of the energy shell; we must attempt to qualify the state as chaotic by exploring all possible partitionings. When applied to the full set of states on the energy shell, this procedure translates into the search for a partitioning that classifies as many states as possible as chaotic. Such a partitioning maximizes f_I.

The maximal $f_I(E)$ obtained in this manner is the proportion of the energy shell occupied by pseudoergodic regions. This quantity is analogous to the classical degree of chaos expressed as the proportion of the energy surface occupied by chaotic trajectories. This procedure for obtaining the "quantum degree of chaos" is somewhat reminiscent of the formal procedure for calculating a rather different measure of classical chaos—the K entropy.[31] However, it is not clear at this point whether this similarity has any deep significance.

Heller has introduced a quantity, denoted by F, which measures the fraction of phase space cells visited by the evolution of a wave packet.[43] This quantity has been suggested as a measure for the degree of ergodicity of quantum systems. Heller's F is, however, rather different from our $f_I(E)$. In terms of the quantities used in our work, the fraction introduced by Heller can be expressed as $C_{A,\mathrm{eq}}/\overline{C}_A(\infty)$, where A are density operators and the correlation functions are defined over a microcanonical ensemble. Although the most general formulation of Heller's theory[29] allows A to be mixed-state density operators, they have been chosen to be pure-state density operators for existing applications.[43] In contrast, the requirement that properties A involved in our calculations be acceptable functions eliminates pure-state density operators from consideration in our work. Furthermore, the quantum behavior is deliberately investigated here for finite times only, using autocorrelation functions that are defined over local distributions in phase space. It is thus difficult to make specific comparisons between our results and those that could be obtained using Heller's procedure.

III. CALCULATIONS

To test the theory presented in last section, we apply it to the quantum Henon–Heiles system and compare the numerically computed results to those obtained classically.

The Hamiltonian for the Henon–Heiles[6] system can be expressed as

$$H=\tfrac{1}{2}(p_x^2+x^2+p_y^2+y^2)+\lambda(xy^2-x^3/3) \tag{33}$$

in Cartesian coordinates, or as

$$H=\tfrac{1}{2}(p_r^2+r^2+p_\theta^2/r^2)-\tfrac{1}{3}\lambda r^2\cos 3\theta \tag{34}$$

in polar coordinates.

We examine the issue of ergodicity for two variants of this system characterized by the values $\lambda=0.1118$ and 0.08. The classical dissociation energy, $D_e=1/6\lambda^2$, for these two cases is, respectively, 13.33 and 26.04. We set Planck's constant $\hbar=1$ in both sets of quantum calculations but, by a familiar scaling argument,[44] the variation of λ can be shown to be equivalent to a variation of $\hbar$ so that the system with the smaller value of λ is more nearly classical than the other one. States for the two systems with different energies E but similar values of E/D_e can be regarded as being in similar classical energy regions. The number of states with energies below D_e is 99 and 374 for $\lambda=0.1118$ and 0.08, respectively.

Eigenvalues and eigenvectors for both systems are obtained by diagonalizing the Hamiltonian in a basis consisting of isotropic harmonic oscillator wave functions satisfying

$$[H_0-(n+1)]|n,l\rangle=0, \tag{35}$$

where H_0 is H of Eq. (33) or (34) with λ set to zero [see Eq. (36a) below].

For the case $\lambda=0.1118$, we use a 903-member basis set that is identical to the one we used in our previous study of the same system.[11] The resulting eigenvalues and matrix elements are well converged. For the case $\lambda=0.08$, we use a 1225-member basis set that is apparently identical to one used by Hose and Taylor[45] in a study of the same system. Although the eigenvalues and matrix elements are not believed to be well converged in this case, we do not expect the ergodic or nonergodic nature of the system to change qualitatively with further improvement of the basis.

Our procedure for detecting the quantum analog of chaos requires calculation of $F_A(\tau)$ for a variety of properties $\hat{A}$. Ideally, of course, we should include in this set all acceptable properties that are "not too strongly localized." In practice, however, we must settle for a manageably small sample of properties and hope that the results of the calculations are effectively converged with respect to this set. In the present investigation, we choose the set of properties to consist of

$$H_0=\tfrac{1}{2}(p_x^2+x^2+p_y^2+y^2), \tag{36a}$$

$$L=(xp_y-yp_x), \tag{36b}$$

$$L^2=(xp_y-yp_x)^2, \tag{36c}$$

$$D=\tfrac{1}{2}(p_x^2+x^2-p_y^2-y^2). \tag{36d}$$

These four properties are selected as being representative of a somewhat larger set that we examined in a previous study.[11] Since these functions are constants of motion for the unperturbed system ($\lambda=0$) they should yield large values of F_A^q for those quantum regions approximately corresponding to classical tori of the unperturbed system. These properties are thus expected to be especially useful for distinguishing between the regular and irregular regions.

Let us return to the question of how small the $F_A^q(\tau)$ must be in order for a quantum region to be judged as pseudoergodic. As discussed in Sec. II, the incomplete relaxation of the time-averaged autocorrelation functions for finite times τ make it impossible to specify a precise theoretical cutoff value for F_A^q which distinguishes chaotic from regular behavior. Changing the cutoff, ϕ, will generally alter the classification of states as ergodic and nonergodic and thus change the computed fraction of irregular states, f_I. Nevertheless, under favorable circumstances an approximate "optimum" value of the cutoff can be determined by examining values of f_I that result from different trial values of ϕ. If the system under consideration behaves in a nearly classical manner and if there is a large difference between the classical F_A values in chaotic and regular regions, then a moderate increase in the cutoff above its optimum value should not substantially change the number of states classified as ergodic and the resulting f_I should remain essentially unchanged. We expect this behavior to contrast with a greater sensitivity of the f_I as the cutoff is varied below and well above the optimum value. Hence, in our calculations, we treat the cutoff value, ϕ, as a parameter. We vary this parameter, repeat calculations of f_I for each such value of ϕ, and attempt to identify the optimum value for the cutoff from the criterion that the f_I be relatively insensitive to these variations.

We now discuss our choice of the value for τ, the observation time used to evaluate the $F_A^q(\tau)$. This choice determines (a) the range about the energy of each ergodic state that must exclude other states that are strongly coupled to it by properties A and (b) the energy separation between states that may be combined to form the superpositions describing pseudoergodic states. The selection of an appropriate value for this time must actually take three factors into account.

One of these imposes a lower limit to τ, while two impose an upper limit. First, the time interval τ must be long enough for the $\overline{C}^q_A(\tau)$ to relax to nearly constant values in pseudoergodic regions. Second, τ must be short enough for the pseudoergodic regions to remain invariant. Finally, τ must be short enough for the purely quantum effects in the $F^q_A(T)$ to be negligible.

Our approach is to choose τ so that the computed f_I is as large as possible for the given cutoff. This procedure tends to ensure satisfaction of both the relaxation and the invariance requirements described above. If τ is chosen to be much shorter than the relaxation time of a given pseudoergodic region, the $F^q_A(\tau)$ for that region will be larger than the cutoff, causing the f_I to be smaller than necessary. On the other hand, if τ is chosen to be larger than the invariance time for the pseudoergodic region, that region will become ineligible as a member of the energy shell partition. The inability to form the optimum partition will again cause f_I to be smaller than its maximum possible value.

This procedure yields 15 and 30 as approximate optimum values of τ for the cases $\lambda = 0.1118$ and 0.08, respectively. These values appear short enough to expect a close correspondence between the quantum and classical behavior during the indicated time scales. Our former calculations[11] for the system with $\lambda = 0.1118$, in fact, showed that there was good agreement between the time-averaged classical and quantum microcanonical autocorrelation functions for times at least as long as 120. Thus, our choices of τ appear likely to obey the requirement that the observation time be short enough for purely quantum effects in the $F_A(T)$ to be negligible. This issue is discussed further in Sec. IV.

The values specified above for τ correspond to only about 2–5 harmonic vibrational periods. Although such times are very short, our calculations show that they are actually long enough for the form of (temporary and local) statistical equilibration needed here to be essentially complete. Previous investigations have shown that the classical, microcanonical autocorrelation functions for the Henon–Heiles system have a rapidly decaying component,[11,46,47] and it is natural to associate this with the relaxation within pseudoergodic zones. The lifetime of this component has been related to the timescale for exponential separation of nearby trajectories (the reciprocal of the maximal Lyapunov number).[46] At the energies considered here, this time scale is in the range 10–30 time units[48] which is, indeed, comparable to our values of τ.

As in our previous work,[11] we express the energy-shell envelope $\rho^\sigma(E - E_J)$ function appearing in F^q_A as a Gaussian function:

$$\rho^\sigma(E - E_J) = \exp[-(E - E_J)^2/2\sigma^2]. \tag{37}$$

The width parameter σ is taken to have the form

$$\sigma/D_e = 0.08 - 0.045E/D_e. \tag{38}$$

In the case $\lambda = 0.1118$, this expression is identical to the one used in our previous work.[11] For both values of λ considered here, Eq. (38) is expected to satisfy the requirements of the energy shell width presented in Refs. 10 and 11.

We perform our calculations for values of E/D_e in the ranges (0.60,0.95) for $\lambda = 0.1118$ and (0.50,0.95) for $\lambda = 0.08$. We restrict the upper limit of these ranges because we wish to avoid energy eigenstates lying far above the dissociation energy. We restrict the lower limit because our previous calculations[11] on the Henon–Heiles system with $\lambda = 0.1118$ showed that classical and quantum microcanonical autocorrelation functions sometimes are in substantial disagreement, even at early times, at energies of $0.44D_e$. This suggests that classical ergodicity is not a meaningful concept for the system at such low energies.

We now turn our attention to the problem of partitioning the states in the quantum energy shell so as to maximize f_I. Finding this optimum partition is equivalent to identifying the operators $\hat{\rho}_n$ that project onto the various portions of the quantum energy shell corresponding to classical pseudoergodic regions. To guide our search for such operators, we consider the topology and nature of the pseudoergodic regions in the classical Henon–Heiles system. At moderately low energies, most of the invariant tori of this system belong to one of two categories[44]: precessing (or circulating) tori bearing trajectories that travel clockwise or counterclockwise around the potential energy surface, and librating (or pendular) tori bearing trajectories that travel back and forth along one of the three C_2 symmetry axes of the potential. As the energy increases and the system becomes progressively more chaotic, most of the tori are destroyed.[6] In many cases, however, trajectories continue, at least for some time, to move over restricted $(2s-1)$-dimensional regions in the vicinity of destroyed s-dimensional precessing or librating tori.[9] The regions of phase space occupied by such trajectories are called vague tori[9] and are examples of ergodic or pseudoergodic regions. Thus, some ergodic and pseudoergodic regions of the Henon–Heiles system resemble precessing and librating tori. However, other ergodic regions of this system may have very complicated topologies with very little resemblence to the simple tori.

The above considerations provide hints concerning the nature of the states $|J\rangle$ that span the pseudoergodic regions and the projectors $|J\rangle\langle J|$ that should be used to form the $\hat{\rho}_n$. Combining these hints with the condition that the $|J\rangle$'s can, at most, be superpositions of nearly degenerate energy eigenstates, leads us to consider the following types of states for the purpose of forming the $\hat{\rho}_n$:

Type A:

$$(1/\sqrt{2})[|a_1\rangle + i|a_2\rangle], \tag{39a}$$

$$(1/\sqrt{2})[|a_1\rangle - i|a_2\rangle], \tag{39b}$$

or

$$|e\rangle, \tag{40a}$$

$$|e^*\rangle. \tag{40b}$$

Type B:

$$(1/\sqrt{3})|a_1\rangle + c(\sqrt{2/3})|e_x\rangle, \tag{41a}$$

$$(1/\sqrt{3})|a_1\rangle - (c/\sqrt{6})|e_x\rangle + (c/\sqrt{2})|e_y\rangle, \tag{41b}$$

$$(1/\sqrt{3})|a_1\rangle - (c/\sqrt{6})|e_x\rangle - (c/\sqrt{2})|e_y\rangle, \tag{41c}$$

or

$$(1/\sqrt{3})|a_2\rangle + c(\sqrt{2/3})|e_y\rangle, \tag{42a}$$

$$(1/\sqrt{3})|a_2\rangle - (c/\sqrt{6})|e_y\rangle + (c/\sqrt{2})|e_x\rangle, \quad (42b)$$

$$(1/\sqrt{3})|a_2\rangle - (c/\sqrt{6})|e_y\rangle - (c/\sqrt{2})|e_x\rangle, \quad (42c)$$

where

$$c = \pm 1. \quad (43)$$

Type C:

$$|a_1\rangle \quad (44)$$

or

$$|a_2\rangle \quad (45)$$

or

$$|e_x\rangle \quad (46)$$

or

$$|e_y\rangle. \quad (47)$$

The energy eigenstates appearing in these equations are classified according to symmetry species A_1, A_2, and E of the C_{3v} point group, as is appropriate for the Henon–Heiles Hamiltonian. In particular, the symbols $|e\rangle$ and $|e^*\rangle$ represent two degenerate, complex, energy states of E symmetry that are related to each other by complex conjugation, while $|e_x\rangle = [|e\rangle + |e^*\rangle]/\sqrt{2}$ and $|e_y\rangle = [|e\rangle - |e^*\rangle]/\sqrt{2}i$ represent the two real, orthogonal superpositions of these states.

Wave functions of type A, described by Eqs. (39) and (40), are complex valued. They are either certain energy eigenfunctions of E symmetry or linear combinations of pairs of real $|a_1\rangle$ and $|a_2\rangle$ energy eigenstates with nearly equal energy ($\Delta E < 1/\tau$). In the limit as $\lambda \to 0$, such type A states become eigenstates[49] of the angular momentum operator L [Eq. (36b)] and correspond to ensembles of classical trajectories precessing in the clockwise [Eqs. (39a) and (40a)] or counterclockwise [Eqs. (39b) and (40b)] sense. For this reason, we suspect that the $\hat{\rho}_n$ constructed out of such $|J\rangle$ may sometimes project onto regions corresponding to vague, classically precessing tori. In these cases, quantum pseudoergodic regions should arise in pairs, corresponding to vague tori with trajectories that circulate in the two senses.

Wave functions of type B, described by Eqs. (41) and (42), are real valued. They are linear combinations of triples of energy eigenstates that lie within a given energy range of width ΔE. The coefficients appearing on the right-hand side of Eqs. (41) and (42) resemble those used to construct sp^2 hybrid orbitals from s, p_x, and p_y orbitals. We thus expect states of type B sometimes to be directionally oriented along the three C_2 axes of the Henon–Heiles potential. (Switching between the choices $c = +1$ or $c = -1$ then simply reverses the directions of the two "lobes" of these states.) This property leads us to suspect that certain states of type B may project onto regions corresponding to vague, classically librating tori. Under these circumstances, quantum pseudoergodic regions should arise in sets of three, corresponding to classical vague tori with trajectories that are oriented along the three C_2 axes.

States of type C, described by Eqs. (44)–(47) are just the uncombined energy eigenstates. Such states may correspond to ergodic classical regions which do not resemble simple precessing or librating tori.

It may seem unlikely that superpositions as primitive as types A and B could accurately describe pseudoergodic regions, even if these regions were vague tori with the expected symmetries. However, it should be noted that our superpositions are directly formed from energy eigenstates, not arbitrary zero-order states. Such energy eigenstates already contain information about the exact dynamics of the system. Thus, these states, even uncombined, are expected to be concentrated mainly in regions of space where the classical motion is restricted during the period of classical-quantum agreement. The principal reason that the uncombined eigenstates fail to represent pseudoergodic regions is, thus, the requirement that they transform as representations of the C_{3v} point group, which causes them to be delocalized over regions associated with more than one symmetrically equivalent vague torus. All that should be necessary, then, to represent the dynamically correct pseudoergodic zones is to adjust the symmetry of the energy eigenstates by forming the simplest superpositions representing distinct, classical, localized distributions.

We now summarize our procedure for identifying pseudoergodic regions and for partitioning the quantum energy shell. We first scan the full energy range of interest for our system and pick out all sets of energy eigenstates with energy spacings that permit formation of type A and type B superpositions. These states and all remaining ones are also candidates for type C states. We then tentatively and arbitrarily assign states of the system to specific allowed types and group together various sets of states of similar types to form "trial" pseudoergodic regions. For each such region consisting of two or more states, we calculate F_A^q for the four properties A previously described. The region is then classified as pseudoergodic if all four of the F_A^q are smaller than the cutoff and as nonergodic otherwise. At that point, it is possible to use Eq. (31) to calculate f_I as a function of energy for this trial partitioning of the states. Finally, it is necessary to repeat the above procedure for each possible assignment of states to the three types and for each different grouping of states to form trial pseudoergodic regions. The choice of type and grouping which yields the largest value of f_I at each energy is accepted as correct.

An aspect of our treatment that may seen puzzling is our identification of pseudoergodic regions with vague tori. This may appear to be inconsistent with semiclassical quantization techniques for chaotic systems which assign specific quantum numbers to certain vague tori. The basic question here is whether the approximate integrals of motion (apart from total energy), associated with these vague tori, really serve to divide the phase space into disjoint regions characterized by distinct quantum numbers. We investigated this issue by generating quantized vague tori using the adiabatic switching procedure. We propagated these vague tori for an additional 30 time units on the fully coupled Henon–Heiles potential with $\lambda = 0.08$, to generate Poincaré surfaces which can be compared to our pseudoergodic regions. We found that although the regions associated with different quantized states occupy somewhat different portions of the Poincaré plane "on the average," these portions seem to overlap substantially when the states under investigation are in the same

ergodic region. We plan to present more details of these and related classical studies elsewhere, but the results described above strongly suggest that there is no conflict between the quantization of states based on vague tori and the formation of a pseudoergodic region by these same tori. The approximate integrals involved in the quantization of vague tori are not sufficiently accurate constants of motion to prevent our condition for pseudoergodicity from being obeyed with a reasonably small value for the cutoff ϕ.

We close this section by mentioning a potential theoretical problem associated with the use of our restricted set of properties A. Since this set does not include the exact integrals of motion for the regular regions of the Henon–Heiles system, a classical calculation, analogous to our present quantum study, would not be able to distinguish between very narrow ergodic and nonergodic regions. Regardless of how small ϕ were chosen, sufficiently narrow nonergodic regions would satisfy $F_A(\tau) < \phi$, for any specified $\tau < \infty$, and would thus be misclassified as ergodic. Consequently, such a classical calculation could, at best, reliably identify only those ergodic regions having a "width" phase space greater than some minimum value, W_m. Since the quantum calculations are, anyway, unable to identify ergodic regions consisting of fewer than two states and since we believe that such regions are wider than W_m for the cases under consideration, we do not consider these restrictions to be important for the current studies. This discussion does, however, indicate that the present set of operators cannot be used to identify ergodic behavior in the Henon–Heiles system as $\hbar \to 0$ unless an auxiliary condition is imposed that specifies a minimum width of W_m for the ergodic regions.

IV. RESULTS AND DISCUSSION

We begin by examining the results for f_I, the proportion of the quantum energy shell occupied by ergodic regions.

In Fig. 1 we consider the case $\lambda = 0.08$ with the observation time τ set to 30. The figure shows curves representing the proportion of the energy shell occupied by *regular* states:

$$f_R(E) = 1 - f_I(E). \tag{48}$$

The various curves represent the calculated results obtained for different values of the cutoff. Each of these curves begins close to unity at low energy and decreases (not always monotonically) as energy is increased.

An important observation is that the f_R curves are relatively insensitive to variations of the cutoff for values of this parameter in the range 0.03–0.05. As discussed in Sec. III, this suggests that a cutoff value near 0.04 is "optimum" for distinguishing chaotic and regular motion. According to this interpretation, the various pseudoergodic and ergodic regions of the *classical* system have values of $F_A(\tau)$ that are distributed mostly over a range between 0.00 and 0.03. As the cutoff is varied within this range, the proportion of classical chaotic states on each energy surface that are correctly identified as irregular changes rapidly from zero (for a cutoff of 0.00) to nearly unity (for a cutoff of 0.03) and so the f_R curves change dramatically. There are relatively few states of any kind—regular or irregular—having values for $F_A(\tau)$ in the range between 0.03 and 0.05. Thus, variation of the cutoff over this range causes only small changes in the f_R curves. Most classical regions having values of $F_A(\tau)$ greater than 0.05 are regular. Thus, increasing the cutoff above this value eventually causes the f_R curves again to vary significantly as regular states are misidentified as chaotic.

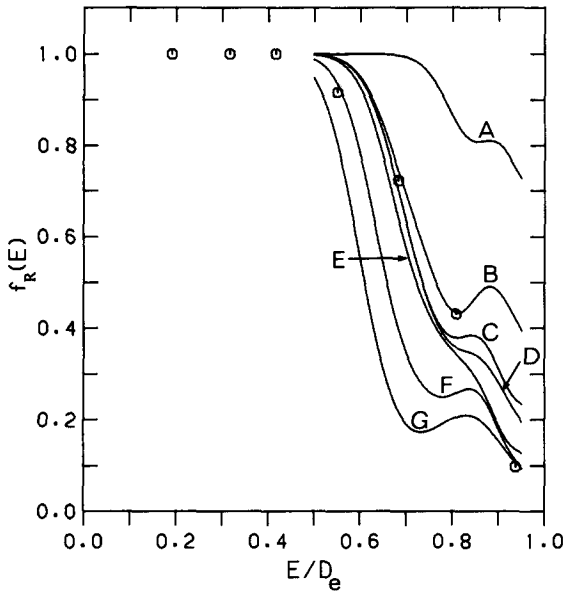

FIG. 1. Proportion of the energy shell occupied by ergodic states for the Henon–Heiles system with $\lambda = 0.08$. The solid curves are quantum mechanical results obtained for $\tau = 30$ with the following values of the cutoff ϕ: (A) 0.01, (B) 0.02, (C) 0.03, (D) 0.04, (E) 0.05, (F) 0.06, (G) 0.07. The circles are the classical results of Powell and Percival, Ref. 8.

A closer look at Fig. 1 reveals that at high energies, $E > 0.85\ D_e$, the f_R curves for cutoffs 0.05 and 0.06 are less sensitive to variations of the cutoff than the curves for 0.03–0.05. This may imply that the optimum cutoff depends on energy. In that case, the optimum cutoff would change from approximately 0.04 for $E < 0.80\ D_e$ to about 0.05 for $E > 0.85\ D_e$.

For the sake of comparison, we note that classical values of the *microcanonical* $F_A(30)$ for our properties A have values that are as large as 0.5 at $E = 0.95\ D_e$.[11] If we had chosen a cutoff of approximately 0.5 in our present calculations, all states at our highest energy range would have been classified as belonging to a single ergodic region consisting of the entire energy shell. Since our optimum cutoff is an order of magnitude smaller, we may expect the corresponding f_R curve to represent very different dynamics and a much finer assignment of ergodic zones on the energy shell. Below, we will see that these expectations are met.

Figure 1 also shows, as circles, the estimates obtained by Powell and Percival[8] for the relative volume of classical energy shells (with width $\sim 0.13 D_e$) occupied by chaotic trajectories. These results are more appropriate for comparison with the quantum f_R curves than are the well-known estimates of Henon and Heiles.[6] The latter authors evaluated the relative area of Poincaré surfaces of section occupied by chaotic trajectories—a quantity that is less directly related to the proportion we measure quantum mechanically.

The quantum f_R curves for the optimum cutoffs of 0.04 (low energy) and 0.05 (high energy) are in generally good

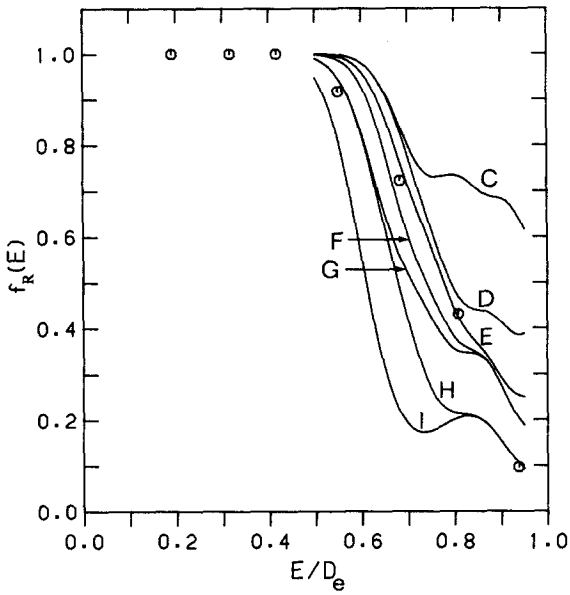

FIG. 2. Same as Fig. 1 but for observation time 15. The cutoff values associated with the curves are as follows: (C) 0.03, (D) 0.04, (E) 0.05, (F) 0.06, (G) 0.07, (H) 0.08, (I) 0.09.

agreement with the classical values. It should be noted that the Powell–Percival results were obtained using an ensemble of only 100 trajectories for the entire energy range $E < D_e$. As a result, the statistical accuracy of their calculation is expected to be limited and small differences between the quantum and classical results may not be significant.

To explore the effects of varying the observation time τ and to help relate the results for $\lambda = 0.08$ to those for $\lambda = 0.1118$, we present, in Fig. 2, $f_R(E)$ curves obtained for the case $\lambda = 0.08$ with $\tau = 15$.

The results shown in this figure are qualitatively similar to those displayed in Fig. 1, but the curves that most closely resemble those of the previous figure are obtained with higher values of the cutoff. This is easily understandable. Decreasing τ causes the $F_A^q(\tau)$ values to increase as a consequence of less complete relaxation of the $\overline{C}_A^q(\tau)$. If the energy and the cutoff are held constant, fewer states are classified as chaotic and f_R increases. To maintain roughly the same values for f_R, the classification criteria for chaos must be relaxed by increasing the cutoff.

The curves in Fig. 2 generally seem to be more sensitive to variations in the cutoff than those of Fig. 1. Although there is still a range of cutoffs (e.g., 0.05–0.07) for which the curves remain relatively unchanged as the cutoff is varied and it is, thus, still possible to identify an approximate optimum value for this parameter, the range of insensitivity is less distinct than in Fig. 1. The more continual variation of the curves with the cutoff suggests that, classically, there is a smaller separation between F_A values for chaotic and regular regions for $\tau = 15$ than for $\tau = 30$.

As in the previous case, the cutoffs yielding the most insensitive curves in Fig. 2 seem to vary with energy, perhaps indicating that the optimum cutoff also is energy dependent. With a little help from Fig. 1, it is possible to argue that the optimum cutoff for $\tau = 15$ varies from 0.04 at low energies ($E/D_e < 0.7$) to 0.07 or even 0.08 at high energies ($E/D_e > 0.8$). However, regardless of whether an artificial f_R curve is constructed to follow such a cutoff path or an actual curve corresponding to any cutoff in the range 0.05–0.07 is selected, the resulting curve is in generally good agreement with the optimum curve obtained from Fig. 1 and with the classical data.

Figure 3 presents $f_R(E)$ curves for the case $\lambda = 0.1118$, and $\tau = 15$. Although there are obvious differences from the $\lambda = 0.08$ results of Fig. 2, there are also some important similarities in the way the curves vary with the cutoff. In both cases, the high energy portions of the curves change significantly when the cutoff is varied from 0.03 to 0.04 and from 0.07 to 0.08. In both cases, curves for cutoffs 0.05 and 0.06 remain close together for the full range of energies while the curve for the cutoff of 0.07 breaks away from the 0.08 curve to join the 0.06 curve at high energy. The degree of similarity between the cutoff dependence of the curves is especially striking in view of the almost fourfold difference in the state density for the two different values of λ considered. These results support our argument that the variation of the curves with the cutoff reflects a purely classical phenomenon.

The differences between Fig. 3 and Fig. 2 are, however, also important. Each f_R curve in Fig. 3 lies above the corresponding one in Fig. 2, indicating a lower ability of the quantum system with $\lambda = 0.1118$ to emulate classical ergodicity and pseudoergodicity. More specifically, the curves for $\lambda = 0.1118$ remain close to unity for significantly higher energies than those for $\lambda = 0.08$. Also, the curves for $\lambda = 0.1118$, with cutoffs above 0.03, turn sharply upwards for $E/D_e > 0.8$ and continue to increase as E/D_e approaches 1.0. Although the curves for $\lambda = 0.08$ also display a tendency to decrease only slowly or even rise at high energy, this form of nonclassical behavior is much stronger in the $\lambda = 0.1118$ case. We will explain these peculiarities later in

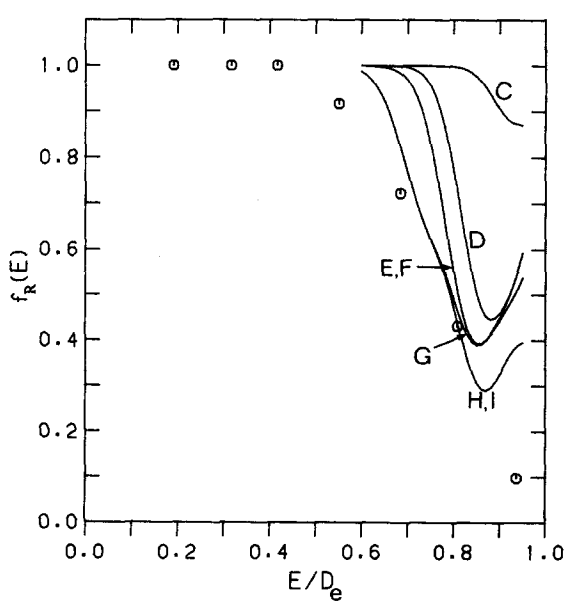

FIG. 3. Same as Fig. 2 but for the system with $\lambda = 0.1118$.

this section, after we have examined the states constituting the ergodic regions.

For the case illustrated in Fig. 3, attempts to use the insensitivity of the f_R curves to determine the optimum cutoff lead to ambiguous results. Successive variations of the cutoff alternately appear to change the curves and leave them unchanged, so that there is now more than one distinct range of cutoffs over which the curves remain constant for much of the energy range. This phenomenon is probably due to the low density of states for $\lambda = 0.1118$. Changes in the f_R occur in discrete units corresponding to the inclusion or exclusion of single states. Since these states are associated with relatively large portions of classical phase space for the present case, the change in the curves with varying cutoffs is more clearly discontinuous. This effectively obscures the rather minor variations in sensitivity in the classical f_R with cutoff that are reflected in Fig. 2 and that must be resolved to identify the optimum value of the cutoff.

Nevertheless, it is again possible to identify an approximate optimum value of the cutoff. Since this value is a classical quantity which does not vary with $\hbar$, it must be the same for the cases illustrated in Figs. 2 and 3. Thus, guided by our conclusions for the case presented in Fig. 2, we continue to accept a value of about 0.06 as the cutoff that best distinguishes chaotic from regular behavior for the present value of λ. We note that the f_R curve corresponding to this cutoff in Fig. 3 is not in good agreement with the classical results. The causes of this discrepancy will be discussed below.

We now examine the partitioning of the quantum states into ergodic and nonergodic regions which yields the optimum curves in Figs. 1 and 3. This division separates quantum states into groups with similar expectation values for properties $\hat{A}$, and thus, similar physical characteristics.

Figure 4 identifies the quantum states forming various ergodic and nonergodic zones for the case $\lambda = 0.08$ with $\tau = 30$ and the cutoff set to 0.04 (cf. curve D of Fig. 1). In this figure, states of the Henon–Heiles system are represented by various symbols at "coordinates" $(n,|l|)$, where n and l are approximate quantum numbers that are assigned to the states in a manner to be described below. Small diamonds denote "nonergodic states" that do not participate in the formation of any ergodic region. Circles represent superposition states of type A (precessing states) formed from A_1 and A_2 energy eigenstates with the same n and $|l|$ or from E states. Chains of circles connected by solid lines represent ergodic regions formed from such states. Each chain of circles actually corresponds to two distinct ergodic regions associated with clockwise and counterclockwise precession. Pairs of boxes connected by dotted lines represent superposition states of type B (librating states) and chains of such pairs connected by solid lines denote ergodic regions spanned by these superpositions. In greater detail, the square box in each pair represents two states of E symmetry while the smaller rectangular box stands for a state of A symmetry. When two rectangles are located at a particular $(n,|l|)$ coordinate, the top one denotes a state of A_1 symmetry while the bottom one represents a state of A_2 symmetry. The single rectangle located at coordinates with $l = 0$ represents a state of A_1 symmetry. Each chain of type B states actually represents three distinct ergodic regions corresponding to librations along the three C_2 axes of the Henon–Heiles potential. No ergodic regions composed of type C states (uncombined energy eigenstates) appear in this figure.

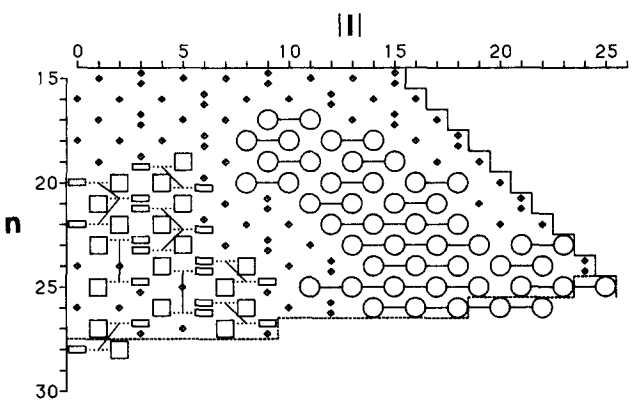

FIG. 4. Ergodic regions of the Henon–Heiles system with $\lambda = 0.08$, obtained for $\tau = 30$ and $\phi = 0.04$. The broken curve at the bottom of the figure separates states above and below the dissociation limit. The remaining symbols are explained in the text.

The n and l values used to label states in Fig. 4 are quantum numbers for eigenstates of the zero-order Hamiltonian H_0. They determine the energy and angular momentum of these states, respectively. Quantum number n can take on values of zero or any positive integer but, for a given n, l is restricted to values of $-n, -n+2,...,n-2, n$. The solid staircase line appearing on the right of Fig. 4 marks the upper bound of the allowed $|l|$ range, $|l| = n$. Values of n and l were assigned to the eigenstates of $\hat{H}$ by comparing the energy eigenvalues to those obtained from the classical second-order perturbative expression for H,[39] by identifying dominant projections of the exact eigenstates onto $\hat{H}_0$ eigenstates, by approximately associating $\hat{L}^2$ expectation values with values l^2, and by examining trends in other matrix elements and in A_1–A_2 energy splittings. Although the assignments are necessarily approximate, they are useful because they allow us to present the partitioning of the states in the illuminating two-dimensional form of Fig. 4. To provide a key to this figure, the energy eigenstates assigned to each $(n,|l|)$ are identified in Table I. We checked these assignments, in selected cases, by comparing the computed energy levels to those obtained by diagonalizing a quantized version[50] of the integrable Jaffe–Reinhardt Hamiltonian[39] and by the adiabatic switching technique.[51,52] Apart from a few exceptions (see Table I), these latter studies confirmed our original assignments. In cases of disagreement, we felt that the original assignments were more credible than those obtained from the semiclassical studies[50–52] since these results then contradicted all remaining evidence for the identity of the states. Note that any reassignment of the states would change the position of certain symbols in Fig. 4 but would not alter the number or type of ergodic regions formed and would have no effect on the results for f_R displayed in Fig. 1.

Some observations regarding Fig. 4 now follow. At the lowest energies (and the lowest values of n) treated, all the states are nonergodic. As the energy is increased, small, precessing ergodic regions first appear for values of $|l|$ that are

TABLE I. Assignment of $(n,|l|)$ quantum numbers for the states of the Henon–Heiles Hamiltonian with $\lambda = 0.08$, represented in Fig. 4.

$(n,\|l\|)$	State
(15, 1)	$41E$
(15, 3)	$25A_1$
(15, 3)	$17A_2$
(15, 5)	$42E$
(15, 7)	$43E$
(15, 9)	$26A_1$
(15, 9)	$18A_2$
(15,11)	$44E$
(15.13)	$45E$
(15,15)	$27A_1$
(15,15)	$19A_2$
(16, 0)	$28A_1$
(16, 2)	$46E$
(16, 4)	$47E$
(16, 6)	$20A_2$
(16, 6)	$29A_1$
(16, 8)	$48E$
(16,10)	$49E$
(16,12)	$21A_2$
(16,12)	$30A_1$
(16,14)	$50E$
(16,16)	$52E$
(17, 1)	$51E$
(17, 3)	$31A_1$
(17, 3)	$22A_2$
(17, 5)	$53E$
(17, 7)	$54E$
(17, 9)	$32A_1$
(17, 9)	$23A_2$
(17,11)	$55E$
(17,13)	$56E$
(17,15)	$33A_1$
(17,15)	$24A_2$
(17,17)	$59E$
(18, 0)	$34A_1$
(18, 2)	$57E$
(18, 4)	$58E$
(18, 6)	$25A_2$
(18, 6)	$35A_1$
(18, 8)	$60E$
(18,10)	$61E$
(18,12)	$26A_2$
(18,12)	$36A_1$
(18,14)	$62E$
(18,16)	$64E$
(18,18)	$39A_1$
(18,18)	$29A_2$
(19, 1)	$63E$
(19, 3)	$37A_1$
(19, 3)	$27A_2$
(19, 5)	$65E$
(19, 7)	$66E$
(19, 9)	$38A_1$
(19, 9)	$28A_2$
(19,11)	$67E$
(19,13)	$68E$
(19,15)	$30A_2$
(19,15)	$41A_1$
(19,17)	$71E$
(19,19)	$74E$
(20, 0)	$40A_1$
(20, 2)	$69E$
(20, 4)	$70E$
(20, 6)	$31A_2$
(20, 6)	$42A_1$
(20, 8)	$72E$
(20,10)	$73E$
(20,12)	$32A_2$
(20,12)	$43A_1$

TABLE I (*continued*).

$(n,\|l\|)$	State
(20,14)	$75E$
(20,16)	$77E$
(20,18)	$34A_2$
(20,18)	$46A_1$
(20,20)	$82E$
(21, 1)	$76E$
(21, 3)	$44A_1$
(21, 3)	$33A_2$
(21, 5)	$78E$
(21, 7)	$79E$
(21, 9)	$45A_1$
(21, 9)	$35A_2$
(21,11)	$80E$
(21,13)	$81E$
(21,15)	$36A_2$
(21,15)	$48A_1$
(21,17)	$85E$
(21,19)	$88E$
(21,21)	$39A_2$
(21,21)	$52A_1$
(22, 0)	$47A_1$
(22, 2)	$83E$
(22, 4)	$84E$
(22, 6)	$37A_2$
(22, 6)	$49A_1$
(22, 8)	$86E$
(22,10)	$87E$
(22,12)	$38A_2$
(22,12)	$50A_1$
(22,14)	$90E$
(22,16)	$91E$
(22,18)	$53A_1$
(22,18)	$41A_2$
(22,20)	$95E$
(22,22)	$99E$
(23, 1)	$89E$
(23, 3)	$51A_1$
(23, 3)	$40A_2$
(23, 5)	$92E$
(23, 7)	$93E$
(23, 9)	$54A_1$
(23, 9)	$42A_2$
(23,11)	$96E$
(23,13)	$94E$
(23,15)	$43A_2$
(23,15)	$56A_1$
(23,17)	$100E$
(23,19)	$103E$
(23,21)	$46A_2$
(23,21)	$60A_1$
(23,23)	$108E$
(24, 0)	$55A_1$
(24, 2)	$97E$
(24, 4)	$98E$
(24, 6)	$44A_2$
(24, 6)	$57A_1$
(24, 8)	$101E$
(24,10)	$107E^a$
(24,12)	$62A_1{}^a$
(24,12)	$49A_2{}^a$
(24,14)	$105E$
(24,16)	$102E^a$
(24,18)	$45A_2{}^a$
(24,18)	$58A_1{}^a$
(24,20)	$111E$
(24,22)	$115E$
(24,24)	$52A_2$
(24,24)	$66A_1$
(25, 1)	$104E$
(25, 3)	$59A_1$

TABLE I (*continued*).

$(n,\|l\|)$	State
(25, 3)	$47A_2$
(25, 5)	$106E$
(25, 7)	$109E$
(25, 9)	$61A_1$
(25, 9)	$48A_2$
(25,11)	$113E$
(25,13)	$110E$
(25,15)	$50A_2$
(25,15)	$64A_1$
(25,17)	$116E$
(25,19)	$118E$
(25,21)	$54A_2$
(25,21)	$69A_1$
(25,23)	$124E$
(25,25)	$128E$
(26, 0)	$63A_1$
(26, 2)	$112E$
(26, 4)	$114E$
(26, 6)	$51A_2$
(26, 6)	$65A_1$
(26, 8)	$117E$
(26,10)	$119E$
(26,12)	$53A_2$
(26,12)	$67A_1$
(26,14)	$121E$
(26,16)	$122E$
(26,18)	$70A_1$
(26,18)	$56A_2$
(26,20)	$127E$
(26,22)	$133E$
...	...
(27, 1)	$120E$
(27, 3)	$68A_1$
(27, 3)	$55A_2$
(27, 5)	$123E$
(27, 7)	$125E$
(27, 9)	$71A_1$
(27, 9)	$57A_2$
...	...
(28, 0)	$72A_1$
(28, 2)	$130E$
(28, 4)	$132E$
(28, 6)	$59A_2$
(28, 6)	$75A_1$
...	...
(29, 3)	$63A_2$
(29, 5)	$142E$

[a] Adiabatic switching and diagonalization of a quantized version of the Jaffe–Reinhardt Hamiltonian suggest the following alternate assignments: $(24,10) = 102E$, $(24,16) = 107E$, $(24,12) = 58A_1$, $(24,18) = 62A_1$, $(24,12) = 45A_2$, $(24,18) = 49A_2$, $(25,11) = 110E$, $(25,13) = 113E$.

somewhat greater than $n/2$. These regions occupy zones somewhat to the right-of-center in the figure but do not extend to the rightmost boundary, defined by $|l| = n$. The states with the highest values of angular momentum thus remain nonergodic. As the energy is increased further, larger precessing ergodic regions appear, extending further to the right-most boundary of the figure, ultimately including even states with the highest allowed $|l|$. Also, at higher energies, librating ergodic regions appear for values of $|l| < n/2$ and occupy zones to the left-of-center in the figure. Although these regions do not include every state with $|l| < n/2$, they do not seem to avoid states with the lowest values of $|l|$ in the same manner as the precessing ergodic regions exclude states with the highest values of $|l|$.

A narrow zone, characterized by $|l| \simeq n/2$, separates the predominantly librating and precessing regions. Most of the states in this intermediate zone are classified as nonergodic. Although not shown in the figure, it is relevant for future discussion to note that the invariance times of ergodic states, as measured by the reciprocal of the separation between energy components in the superpositions, generally increase as one moves away from this central nonergodic strip. Ergodic states nearest this strip have very short invariance times (as low as 30 time units) while those toward the right and left boundaries of the figure tend to have very long invariance times (up to several thousand units). As previously discussed, such times may correspond to classical lifetimes of pseudoergodic zones in certain cases but may represent maximum time scales of good classical-quantum correspondence in others.

Most of the above observations can be explained as straightforward reflections of the manner in which chaos appears in the classical Henon–Heiles system. To see this, let us review the development of chaos in the classical system. At low energies, the vast majority of trajectories are regular and lie on invariant tori. There are two different kinds of trajectories[44]: those with high angular momentum executing precessing motion and those with low angular momentum undergoing librating motion. The phase space surface separating the regions associated with the different kinds of motion is called the precessor–librator separatrix.[53] At these low energies, the most significant, but still very narrow, zone of chaos lies near the separatrix. As the energy is increased, the chaotic region around the separatrix broadens. However, this region is still limited in extent to intermediate values of the angular momentum and trajectories with high and low angular momentum remain regular. As the energy is raised further, the chaotic zone surrounding the separatrix continues to broaden, with regions of lowest angular momentum becoming chaotic before regions of highest angular momentum.[54] Finally, at energies near D_e, the vast majority of the trajectories become chaotic. It is, however, important to note that, even at energies near D_e, a large proportion of the chaotic trajectories tend to remain in regions resembling tori (vague tori) for various periods of time.[9] Such trajectories temporarily execute motion that is qualitatively similar to either regular precessions or librations, depending on the initial values of the angular momentum. It is expected (but, as far as we are aware, not yet demonstrated) that the length of time that these trajectories undergo such restricted motion (i.e., the "lifetime" of the vague tori) generally increases as one moves away from the separatrix to regions of high and low angular momentum.

To relate this description to Fig. 4, we merely identify the classical vague tori with the quantum pseudoergodic regions. We then find that our discussion of classical chaos provides an explanation of various phenomena appearing in this figure, including the forms, positions, and patterns of the pseudoergodic regions. The classical description is (perhaps fortuitously) even consistent with the observed trends in the invariance times of the pseudoergodic zones. How-

ever, this discussion raises questions about the central nonergodic strip. Since this strip separates regions of librating from precessing motion, it must correspond to the zone around the separatrix. This zone is, however, the most chaotic portion of phase space. The lack of ergodicity in this quantum region is therefore disturbing. Below, we review an investigation we carried out to understand this result.

A possible explanation for our inability to find ergodicity in the central strip is that, although ergodic regions are present in that zone, relaxation to a statistical equilibrium distribution is much slower than for other portions of phase space. Thus, detection of ergodic regions in the central strip requires evaluation of F_A^q for values of τ that are substantially larger than 30. Use of a larger value of τ for these cases can easily be rationalized if these regions are spanned by different types of states than those forming the precessing and librating regions, e.g., uncombined energy eigenstates (type C states). To investigate this possibility, we chose a value of $\tau = 120$ for regions potentially spanned by type C states. We found that, indeed, a few states in the central strip, previously classified as nonergodic, now formed type C ergodic regions. When we further increased τ to 300 we not only detected a few additional regions of this kind, but found that maximization of f_I required formation of type C regions from states identified as part of type A and B regions in Fig. 4.

Although these results appeared promising, the ergodic regions in the central strip did not seem to correspond to portions of phase space with well-defined classical analogs. Of the eight new ergodic regions found with $\tau = 300$ and a cutoff of 0.04, seven were composed solely of states with A_1 and A_2 symmetry and one was composed solely of states with E symmetry. The different propensity of states with different symmetry to form ergodic regions and the tendency of ergodic regions formed from states with different symmetry to remain separate are nonclassical effects. As $\hbar \to 0$, the smoothed density functions obtained from energy eigenstates of different symmetry become indistinguishable. Thus, in the classical limit, there can be no distinction between the phase space regions formed from states of A and E symmetry.

Another possible explanation for the absence of ergodic regions in the central strip of Fig. 4 is that such regions must be constructed from as-yet unexplored superpositions of energy eigenstates, i.e., superpositions of types other than A and B. These ergodic regions would, of course, have to remain invariant for long enough periods of time for relaxation to be complete. However, a scan of energy differences shows that there are only three possible, new, superpositions that can be formed in the central strip with invariance times greater than 1 time unit and the longest of these times is only about 10 units (approximately 1.5 harmonic vibrational periods). Complete relaxation on such short time scales seems unlikely.

More generally, we find that with only two exceptions for all the states in Fig. 4, the superpositions of type A and B combine energy eigenstates with the smallest energy separations. Any new superpositions would represent regions that are invariant for even shorter times than those we have already considered. Therefore, apart from the type C regions, there are almost no candidates to represent new ergodic regions that might be formed once type A and B regions break up.

The absence of ergodic behavior in the quantum central strip is probably due to the instability[1,2] of the classical motion near the separatrix. As a result of this instability, any vague tori that may appear in this strip are so short lived that relaxation within these regions is incomplete. Thus, temporarily ergodic regions are not formed near the separatrix. On the other hand, relaxation over larger portions of phase space to form true ("permanently") ergodic regions is so slow that the times involved exceed the time scale of good classical-quantum agreement. The reason for the slowness of this relaxation is that it requires passage of phase space density across significant bottlenecks associated with the presence of vague tori. It is only when these vague tori break up (and the pseudoergodic regions lose their invariance) that a permanent form of relaxation is complete.

The following conclusions thus emerge from this study: (a) the central strip really does appear to be nonergodic insofar as quantum dynamics is concerned; (b) there is no convincing evidence of the formation of ergodic regions of type C for our system; (c) the time scale for classical-quantum correspondence in our system is shorter than 120 time units. The last conclusion results from the observation that the new ergodic regions appearing for $\tau = 120$ are nonclassical in nature.

Throughout our investigation we have anticipated that classical chaos can be reflected in quantum dynamics in the form of ergodic-like behavior only if the classical ergodic relaxation is complete prior to the breakdown of quantum-classical agreement. Indeed, this principle underlies the semiclassical ergodic theory.[10] What is surprising about our results is the extreme shortness of the time scale for quantum-classical agreement, even for a relatively "classical" model. The very limited period for similarity of the two dynamics seems to prevent the quantum system from exhibiting ergodicity over the full region that it is attained in the classical counterpart.[6]

Our observation of short times for classical-quantum agreement is consistent with results very recently reported by Brown and Wyatt[55] for a model system describing multiphoton dissociation. These authors found that quantum density prepared in a classically chaotic region was unable to cross a classical bottleneck as quickly as in the classical case. This result can be interpreted as an indication that the classical invariance time of the region bounded by the bottleneck is longer than the time scale for agreement between classical and quantum dynamics. It is the resulting failure of quantum mechanics to describe the classical diffusion across bottlenecks that is responsible, in the present system, for the lack of ergodicity over large classical regions.

The short time period for correspondence appears to be inconsistent with our previous investigations[11] which show that classical and quantum *microcanonical* autocorrelation functions are in good agreement for times of at least 120 units, even for the more quantum mechanical case of $\lambda = 0.1118$. However, we must bear in mind that the present

results are related to the behavior of autocorrelation functions that are rather different than those investigated previously. Our present autocorrelation functions probe the dynamics in very small regions in phase space, not the full energy shell, and evidently tax the classical-quantum correspondence to a far greater extent than before.

We now discuss the states with $|l| \simeq n$ and $|l| \simeq 0$, which are identified as nonergodic by our analysis. Our classification of these states is consistent with the findings of other authors. For example, Davis, Stechel, and Heller[56] showed that a wave packet prepared in a classically nonergodic, precessing region of the Henon–Heiles system (with $\lambda = 0.1118$) projected almost exclusively onto a certain set of energy eigenstates. Examination reveals these states to be just our high $|l|$ nonergodic states. Hose and Taylor[28] concluded that these same high $|l|$ states arise from classical quasiperiodic motion since the absolute square of their projections onto specific eigenstates of a separable Hamiltonian exceeds 0.5. The separable Hamiltonian used to test these states was our H_0 and the states qualifying as quasiperiodic in this manner were called "Q^{I}" states. In a similar way, another separable Hamiltonian was used to classify some of the lowest $|l|$ states as quasiperiodic and these were called "Q^{II}" states. The general quasiperiodic classification of such extreme-motion states was later explained by Taylor and coworkers[57] on the basis of the adiabatic principle. However, despite the above remarks, there does not appear to be truly consistent agreement between extreme-motion states identified as nonergodic by the present analysis and those classified as Q^{I} or Q^{II} by the original Hose–Taylor prescription. For example, although the Hose–Taylor criterion classifies the high $|l|$ states of the system with $\lambda = 0.1118$ as Q^{I}, it does not classify the analogous states of the system with $\lambda = 0.08$ as Q^{I},[45] although our analysis shows both sets of states to be nonergodic. Of course, it is possible that agreement between our classification and that of Hose and Taylor may be achieved by applying their criterion with other choices for the separable Hamiltonian.

Let us briefly consider the mechanism responsible for the formation of ergodic regions in our quantum system. Since a characteristic of these regions is that the constituent states have similar physical properties, one might expect all such states in an ergodic region to be superpositions of the same zero-order states and the mechanism for their formation to be simply the mutual coupling of the unperturbed states in these zones. A glance at Fig. 4, however, immediately shows that this expectation is incorrect and that the proposed mechanism is, at best, incomplete. Consider, for example, one of the librating ergodic regions consisting of states $(n = 17,\ |l| = 9)$ and $(n = 17,\ |l| = 11)$ [e.g., $32A_1 + i(23A_2)$ and $55E$; see Table I]. Since the two states in this region are of different symmetries and are obtained by diagonalizing separate blocks of the Hamiltonian, they are necessarily superpositions of different zero-order states. The mechanism causing such states to have similar physical properties must be more general than the interaction between states of the same symmetry and, in fact, must transcend purely quantum symmetry considerations. It appears that such a mechanism must, in some way, rely on the correspondence principle and the behavior of the system in the classical limit.

Before leaving Fig. 4, we must comment on the reliability of certain features appearing there. Ideally, all of the boundaries separating the different ergodic zones in Fig. 4 should correspond to classical bottlenecks in phase space. However, the quantum boundaries in the high-energy, librating portion of the figure are subject to large uncertainties, so that they may not always accurately reflect the classical division of phase space. The uncertainties arise because the sizes and shapes of the high-energy, librating ergodic regions are rather sensitive to variations of the cutoff. Although the number and identity of the ergodic states do not change significantly as the cutoff is varied by small amounts about its optimum value, the form of the ergodic zones do. Thus, if ϕ is taken to have the value 0.05 at high energy (a choice that we have previously justified) it becomes possible to form librating ergodic regions containing as many as four states and involving both $A_1 - E$ and $A_2 - E$ superpositions. As a result, the high energy librating ergodic zones may not be quite as small as they appear in Fig. 4 and, in contrast to the implication of that figure, there may be a tendency for these zones to become larger as energy is increased, as in the precessing case.

We now turn our attention to the case $\lambda = 0.1118$, $\tau = 15$. Figure 5 shows the partitioning of the quantum states that corresponds to the optimum cutoff of 0.05–0.06 (cf. curve E,F in Fig. 3). The assignment of zero-order quantum numbers to the states of this system is taken from the work of Jaffe and Reinhardt.[39]

In many ways, this figure resembles Fig. 4: at suitably high energies, states with low $|l|$ form librating ergodic regions, those with high $|l|$ form precessing ergodic regions, while those with the highest $|l|$ tend to form nonergodic regions. However, this figure differs significantly from Fig. 4 in that proportionally fewer states fall into ergodic regions. Many states that are classified as nonergodic in Fig. 5 correspond to states that lie in ergodic regions of Fig. 4. Root mean square energy deviations obtained in adiabatic switching studies[51,52] verify that such "missing" ergodic states in Fig. 5 are indeed located in classical chaotic regions.

These missing ergodic states explain the different appearance of the optimum f_R curves for the two values of λ. The relatively small number of ergodic states for $n < 11$ in the $\lambda = 0.1118$ case is responsible for the tendency of curve C in Fig. 3 to remain near unity until energies above $0.7\,D_e$.

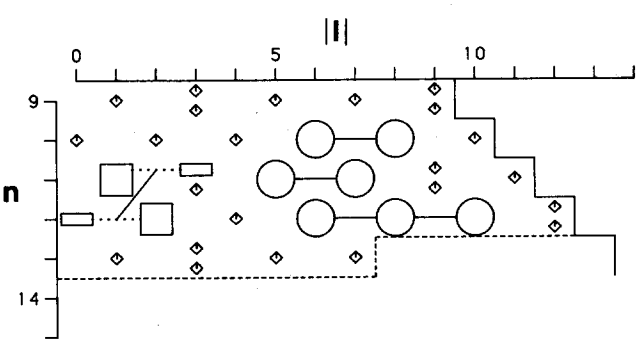

FIG. 5. Same as Fig. 4 except that $\lambda = 0.1118$, $\tau = 15$, and $\phi = 0.05$–0.06.

The absence of ergodic states in the last row of Fig. 5 is responsible for the sharp upturn in curve C at energies above $0.85\,D_e$.

The reason for the missing ergodic states in Fig. 5 is the small size of the ergodic regions in the classical limit. The states missing in Fig. 5 are mostly those that would belong to ergodic zones composed of only two or three states in Fig. 4. In passing from $\lambda = 0.08$ to $\lambda = 0.1118$, however, the number of quantum states in a fixed region of phase space associated with a vague torus decreases by a factor ranging from about $2[\simeq (0.1118/0.08)^2]$ to about $4[\simeq (0.1118/0.08)^4]$, depending on the shape of the region. Since our treatment automatically classifies regions containing fewer than two states as nonergodic, only those ergodic zones consisting of many states for $\lambda = 0.08$ remain ergodic for $\lambda = 0.1118$.

Nonergodic zones, similar to the one observed in Fig. 5 for low $|l|$ and high energy, have been found in analogous regions of phase space in other classically chaotic quantum systems.[22] Quantum systems, prepared in such zones, remain trapped there for long periods of time while the corresponding classical systems may quickly leave these regions, undergo substantial intramolecular energy transfer, and dissociate. It is possible that the mechanism inhibiting the ergodic behavior of these systems is similar to the one apparently at work here: the division of classical phase space into narrow pseudoergodic regions by a dense distribution of bottlenecks.

We have already noted that the f_R curves for $\lambda = 0.08$ (Fig. 1) also display some of the nonclassical features found for $\lambda = 0.1118$ (Fig.3), albeit to a much smaller extent. As in the latter case, this nonclassical behavior may be due to the small size of classical pseudoergodic regions. The crucial point is, however, that the discrepancies between the classical and quantum values for f_R do become much less pronounced as λ becomes smaller. The tendency for the classical and quantum degrees of chaos to become more similar suggests that the influence of these small regions rapidly becomes negligible as $\hbar$ is decreased and supports the validity of our approach for identifying the quantum manifestations of chaos.

It is of some interest to compare our present conclusions regarding the ergodicity of the Henon–Heiles system with those arising from an earlier investigation. In a previous calculation,[11] we observed that the microcanonical versions of the classical and quantum functions $F_A(T)$ for the Henon–Heiles system were in good mutual agreement for the case $\lambda = 0.1118$ and $E = 0.95\,D_e$. Thus, as measured by that test, the quantum system displayed the same degree of ergodic behavior as the classical system. In the present calculation, however, we appear to arrive at just the opposite conclusion: as measured by the current test, the quantum Henon–Heiles system exhibits a much lower degree of ergodic behavior than its classical counterpart.

This apparent paradox is resolved by recognizing that the form of ergodicity probed in the earlier work was global ergodicity, whereas the kind of ergodicity we examine here is local pseudoergodicity. The present form of ergodicity is more strictly obeyed by the classical system and is a more reliable indicator of chaotic behavior.

This does not, however, mean that the results established here are necessarily more relevant for applications than those obtained previously. Indeed, our former conclusions have direct implications for theories that require statistical equilibration on the full energy surface. They suggest, for example, that the RRKM requirement of intramolecular randomization is likely to be satisfied to the same extent by the quantum Henon–Heiles system at $E = 0.95\,D_e$ as by the corresponding classical system. On the other hand, our present results are relevant to more recent and more detailed statistical theories that require local pseudoergodicity.[37,38] Thus, for example, our work suggests that the classical theory of intramolecular relaxation proposed by Davis[38] might not be easily generalizable to the current quantum system at high energy.

V. SUMMARY AND CONCLUSIONS

We have attempted to identify a form of quantum dynamical behavior that is a direct consequence of the chaos in the corresponding classical system. Since agreement between classical and quantum dynamics generally deteriorates for long observation times, we have sought a classical characteristic property that could be used to identify chaos even over short observation periods. This property is local, nontrivial, pseudoergodicity.

We have examined the semiclassical analog of pseudoergodicity, the conditions under which a quantum system can be expected to exhibit this form of behavior, and the relationship between this property and the underlying classical chaos. We have concluded that the quantum states that lie in the analog of a classical pseudoergodic region are generally superpositions of energy eigenstates. All such states in a given region have similar expectation values for operators that are acceptable and not too highly localized. Furthermore, off-diagonal matrix elements of these operators between states in a pseudoergodic region and all other states of similar energy are small. The degree to which these conditions are satisfied can be determined by examining the values of $F_A(\tau)$ for the various operators A.

We have applied this analysis to the Henon–Heiles system with two choices for the nonlinearity parameter λ. To judge the degree to which classical chaos is reflected in the quantum dynamics, we have compared the proportion of the quantum energy shell occupied by pseudoergodic regions to the proportion of the classical energy shell occupied by chaotic trajectories. To further check our identification of the quantum analog of pseudoergodicity, we have examined the quantum states participating in ergodic regions and related them to classical pseudoergodic zones.

For the version of the Henon–Heiles system with the lower value of λ we have found good agreement between the classical degree of chaos and the corresponding quantum measure but for the version with the higher value of λ we have found much poorer agreement. We have explained this trend to be a consequence of the more quantum mechanical nature of the latter system and the smaller size of the classical ergodic zones relative to h^s.

Our investigation has shown that, even at high energy,

the quantum energy shell is divided into several disjoint pseudoergodic zones that are separated by what appear to be quantum analogs of the precessor–librator separatrix and other classical bottlenecks. Superposition states spanning librating and precessing pseudoergodic zones are those that would be expected to represent librating and precessing tori when the classical dynamics of the Henon–Heiles system is regular. We have, therefore, identified these pseudoergodic zones as the analogs of vague tori.

Despite these results, however, a major conclusion of our work is that classical chaos does not always show up as ergodic-like behavior of the analogous quantum system. Thus, even when the classical motion underlying a quantum state is chaotic, such a state need not belong to a quantum ergodic or pseudoergodic zone. For the chaotic motion to influence the quantum dynamics in an identifiable way, the associated ergodic or pseudoergodic region must be sufficiently large (consisting of two or more quantum states) and the statistical relaxation in that region must be sufficiently fast (faster than the breakdown of the quantum-classical agreement). Indeed, our work has suggested that the necessary time scale for relaxation is so short, even for fairly "classical" quantum systems, that it is pseudoergodicity, rather than true ergodicity, that is generally reflected in the quantum behavior of a classically chaotic system. Our calculations have not produced evidence of quantum behavior that is analogous to true, "permanent" ergodicity over large portions of the energy surface, such as is achieved in the classical Henon–Heiles system at high energy.[6]

We conclude with a brief discussion of some difficulties that may hinder routine application of our treatment to other systems.

An important practical problem with our approach concerns the choice of the operators A that are used to test for ergodicity. In principle, one should consider all operators that are acceptable and that are not too strongly localized. Although a "complete" set of such operators can be defined and this set is finite for nonzero $\hbar$, it is too large to permit actual computations on systems such as the Henon–Heiles model with $\lambda = 0.08$. An alternative procedure is to select a small number of operators that are expected to be most efficient at identifying states that are nonergodic. Such operators are those that correspond to approximate classical constants of motion for the system. In this paper we have adopted this approach, choosing the set of A to consist of simple operators that commute with the zero-order Henon–Heiles Hamiltonian. A more systematic procedure would be to select operators that correspond to the approximate action variables produced by classical perturbation theory.[39] Although this approach requires rather difficult calculations it appears to be worthy of further investigation.

Another problem that obstructs application of our method to other systems is the difficult task of finding the optimal partitioning of states in the energy shell into pseudoergodic regions, in order to maximize $f_I(E)$. In the present work, this process was carried out manually in a trial-and-error manner. Of course, the same procedure can be applied to systems with moderate state densities. However, this approach is tedious, subject to human error and in any event, impractical for systems with truly high state densities. Though not a simple task, development of an efficient, intelligent algorithm for this step is not impossible for systems with finite state densities, and would make the routine application of our method much simpler.

The problem of forming the correct superpositions $|J\rangle$ to represent pseudoergodic zones for other systems may not be as severe as first appears. Given information about the topology of classical vague tori, our experience suggests that considerations of symmetry and energy level spacings often uniquely determine the appropriate linear combinations. Indeed, there is evidence that vague tori in symmetric triatomic systems have topologies similar to the librating and precessing pseudoergodic regions of the Henon–Heiles case.[58] Thus, the states $|J\rangle$ for such systems should bear a close analogy to the superpositions formed in our present work. It should also be noted that our results do not rule out the possibility that uncombined energy eigenstates suffice to represent pseudoergodic regions for systems without symmetry. If that is true, the problem of forming the correct superpositions never arises for such cases.

As this discussion suggests, successful treatment of other systems by the approach presented in this paper may require rather thorough preliminary studies of both the classical and quantum dynamics. Such investigations are needed to compensate for the inability to consider all appropriate operators A and to overcome the uncertainties concerning the correct choice of the superposition states $|J\rangle$. Ideally, these studies should provide information about the topology of the regular and the irregular (pseudoergodic) regions of classical phase space, the good classical action variables, and the shapes of the stationary wave functions. In the case of the Henon–Heiles system, we were able to draw on the wealth of results from previous investigations. Treatment of other systems may require additional calculations.

Finally, we mention that we have recently carried out classical calculations of local ergodicity analogous to those presented in this paper. These calculations corroborate many of the claims we have made regarding the classical interpretation of our work. We plan to present full details of these investigations elsewhere.

ACKNOWLEDGMENTS

We thank Mr. S. W. Cho for making available to us the computer programs used for the adiabatic switching calculations. We thank the reviewer for making several constructive suggestions. This research was supported by National Science Foundation Grant CHE-8418170.

APPENDIX A: SUPPLEMENTARY APPROXIMATE INTEGRALS OF MOTION

Systems with more than two degrees of freedom often have approximate, isolating, constants of motion that temporarily confine the classical chaotic dynamics to regions of phase space with lower dimensionality than the full energy surface.[40–42] In this Appendix we discuss the modifications to the theory presented in Sec. II that are needed when this restriction of the motion persists for periods exceeding the

time range of good classical-quantum agreement.

Let us assume that the chaotic motion is subject to a total of $m < s$ isolating constants of motion $I_1, I_2, \ldots, I_m$, where s is, as usual, the number of degrees of freedom of the system. Some of these constants may be exact integrals (e.g., the total energy) while others may be approximate constants. Then the motion will be temporarily restricted to a region in phase space of dimensionality $2s - m$ and we must redefine nontrivial (pseudo)ergodicity to refer to (temporary) ergodic behavior in such regions.

This new definition requires only two modifications of the classical ergodicity conditions presented in Sec. II: (a) the Dirac delta function $\delta(E - H)$ appearing in the classical density function $\rho(\mathbf{p},\mathbf{q})$ must be replaced by the multidimensional delta function $\delta(\mathbf{I} - \mathbf{I}')$ that projects onto the restricted portion of phase space associated with the motion; (b) the properties A that are used to test for ergodicity must now exclude all functions depending only on $\mathbf{I}$, since these lead to indeterminate values of F_A.

The modifications needed in the quantum conditions are analogous to those described above: (a) The expression for the quantum density operator $\hat{\rho}$, presented in Eq. (18) must be replaced by

$$\hat{\rho} = \sum_J{}' |J\rangle \rho^\sigma(\mathbf{I}^J - \mathbf{I}') \langle J|, \tag{A1}$$

where $\mathbf{I}^J$ is a vector of expectation values $\langle J|\mathbf{I}|J\rangle$ for operators $\hat{I}$ corresponding to the classical constants of motion, and $\rho^\sigma(\mathbf{I}^J - \mathbf{I}')$ is a product of m decreasing functions of $|I_i^J - I_i'|$ (e.g., Gaussians); (b) the operators $\hat{A}$ for which F_A are evaluated must now exclude all functions depending only on $\mathbf{I}$.

Modifications such as these allow one to identify the semiclassical analog of ergodicity for regions of any dimensionality. In particular, if m is permitted to be equal to s, the considerations described above lead to a semiclassical definition of trivial ergodicity.

APPENDIX B: INVARIANCE AND SUPERPOSITION STATES $|J\rangle$

Here we examine the consequences of the invariance requirement for the choice of states $|J\rangle$. The effective invariance of $\hat{\rho}$ over the time period $0 \leqslant T \leqslant \tau$ implies that

$$\begin{aligned}\hat{\rho}(T) &= \exp(-iHT/\hbar)\hat{\rho}\exp(iHT/\hbar) \\ &= \rho(0) \quad \text{for} \quad 0 \leqslant T \leqslant \tau.\end{aligned} \tag{B1}$$

Substituting Eq. (18) for $\hat{\rho}$ into this expression, we get

$$\begin{aligned}\hat{\rho}(T) = \sum_J{}' &\exp(-iHT/\hbar)|J\rangle \rho^\sigma(E - E_J)\langle J| \\ &\times \exp(iHT/\hbar).\end{aligned} \tag{B2}$$

Introducing complete sets of exact energy eigenstates (denoted by lower-case letters within bras and kets) into the above expression, we obtain

$$\begin{aligned}\hat{\rho}(T) = \sum_J{}' \sum_k \sum_l &|k\rangle\langle k|J\rangle \\ &\times \rho^\sigma(E - E_J)\langle J|l\rangle\langle l|\exp(i\omega_{lk}T),\end{aligned} \tag{B3}$$

where $\omega_{lk} = (E_l - E_k)/\hbar$. Thus, the requirement that $\hat{\rho}(T) = \hat{\rho}(0)$ for $T \leqslant \tau$ yields

$$\begin{aligned}\sum_J{}' \sum_k \sum_l &|k\rangle\langle k|J\rangle \rho^\sigma(E - E_J)\langle J|l\rangle\langle l|\exp(i\omega_{lk}T) \\ &= \sum_J{}' \sum_k \sum_l |k\rangle\langle k|J\rangle \rho^\sigma(E - E_J)\langle J|l\rangle\langle l|.\end{aligned} \tag{B4}$$

We conclude that, in order for $\hat{\rho}(T)$ to remain invariant for $T \leqslant \tau$, the spacings between the energy levels of those eigenstates that project onto each state $|J\rangle$ must be small enough that $\omega_{lk} T \ll 1$ for $T \leqslant \tau$. This condition will be satisfied if each state $|J\rangle$ is composed only of energy eigenstates that are close in energy. More specifically, if ΔE is the largest energy separation between two energy components of $|J\rangle$, we demand that

$$\Delta E\, T/\hbar \ll 1 \quad \text{for} \quad T \leqslant \tau, \tag{B5}$$

i.e.,

$$\tau < \hbar/\Delta E. \tag{B6}$$

APPENDIX C: EXPRESSION FOR $F_A^q(\tau)$

We now derive an explicit formula for $F_A^q(\tau)$. Equation (14) expresses $F_A^q(\tau)$ in terms of the time averaged autocorrelation function $\bar{C}_A^q(\tau)$ and its statistical equilibrium value $C_{A,\text{eq}}^q$. To evaluate $\bar{C}_A^q(\tau)$ we apply the definition

$$\bar{C}_A^q(\tau) = D_A^{-1}(1/\tau)\int_0^\infty dt \exp(-t/\tau)\langle A(t)|A\rangle^q, \tag{C1}$$

where

$$\begin{aligned}\langle A(t)|A\rangle^q &= \mathrm{Tr}[\hat{\rho}\hat{A}(t)^\dagger \hat{A}] \\ &= \sum_J{}' \rho^\sigma(E - E_J)\langle J|A(t)A|J\rangle\end{aligned} \tag{C2}$$

and

$$D_A = \langle A|A\rangle^q. \tag{C3}$$

Introducing complete sets of exact eigenstates (denoted by lower-case letters) and superposition states (denoted by capital letters) into these expressions, we obtain

$$\begin{aligned}\langle A(t)|A\rangle^q &= \sum_J{}' \sum_K \rho^\sigma(E - E_J)\langle J|A(t)^\dagger|K\rangle\langle K|A|J\rangle \\ &= \sum_J{}' \sum_K \sum_n \sum_m \rho^\sigma(E - E_J)\langle J|n\rangle\langle n|A^\dagger|m\rangle \\ &\quad \times \langle m|K\rangle\langle K|A|J\rangle \exp(i\omega_{nm}t)\end{aligned} \tag{C4}$$

and

$$D_A = \sum_J{}' \rho^\sigma(E - E_J)\langle J|A^\dagger A|J\rangle. \tag{C5}$$

Sufficiently near the classical limit, and with an appropriately large value of σ, the imaginary parts of $\langle A(t)|A\rangle^q$ and $\bar{C}_A^q(\tau)$ are negligible for real functions $A(p,q)$, and we can replace $\bar{C}_A^q(\tau)$ by $\mathrm{Re}\{\bar{C}_A^q(\tau)\}$. Thus, substituting Eq. (C4) into Eq. (C1), integrating, and taking the real part, we obtain

$$\hat{C}_A^q(\tau) = D_A^{-1} \sum_J{}' \sum_K \sum_n \sum_m \rho^\sigma(E - E_J)\langle J|n\rangle\langle n|A|m\rangle$$

$$\times\langle m|K\rangle\langle K|A|J\rangle/[1+(\omega_{nm}\tau)^2]. \quad \text{(C6)}$$

By construction, the only nonzero terms in the sum are those that satisfy $E_J \approx E_n$ and $E_K \approx E_m$ where $E_J = \Sigma_n E_n |\langle J|n\rangle|^2$ and $E_K = \Sigma_n E_n |\langle K|n\rangle|^2$. Hence, $\omega_{nm} \approx \omega_{JK} = (E_J - E_K)/\hbar$. Taking this into account, we get

$$\overline{C}^q_A(\tau) = D_A^{-1} \sum_J{}' \rho^\sigma(E-E_J) \sum_K |\langle J|A|K\rangle|^2 / [1+(\omega_{JK}\tau)^2]. \quad \text{(C7)}$$

Similarly, we obtain the following expression for $C^q_{A,\mathrm{eq}}$:

$$C^q_{A,\mathrm{eq}} = \left[\sum_J{}' \rho^\sigma(E-E_J)\langle J|A|J\rangle\right]^2 \Big/ \left\{D_A\left[\sum_J{}' \rho^\sigma(E-E_J)\right]\right\}. \quad \text{(C8)}$$

Substituting these results into the expression for $F^q_A(\tau)$ in Eq. (14) and rearranging, we obtain the result presented in Eq. (23).

[1] A. J. Lichtenberg and M. A. Lieberman, *Regular and Stochastic Motion* (Springer, New York, 1983).

[2] Reviews include B. V. Chirikov, Phys. Rep. **52**, 263 (1979); P. Brumer, Adv. Chem. Phys. **47**, 117 (1981); M. V. Berry, in *Topics in Nonlinear Dynamics*, edited by S. Jorna (AIP, New York, 1978); D. W. Noid, M. L. Koszykowski, and R. A. Marcus, Annu. Rev. Phys. Chem. **32**, 267 (1981).

[3] R. Balescu, *Equilibrium and Nonequilibrium Statistical Mechanics* (Wiley–Interscience, New York, 1975).

[4] Cases in which there are exact or approximate integrals of motion in addition to the total energy are treated in Appendix A.

[5] I. E. Farquhar, *Ergodic Theory in Statistical Mechanics* (Interscience, London, 1964).

[6] M. Henon and C. Heiles, Astron. J. **69**, 73 (1964).

[7] H.-D. Meyer, J. Chem. Phys. **84**, 3147 (1986).

[8] G. B. Powell and I. C. Percival, J. Phys. A **12**, 2053 (1979).

[9] R. B. Shirts and W. P. Reinhardt, J. Chem. Phys. **77**, 5204 (1982).

[10] K. G. Kay, J. Chem. Phys. **79**, 3026 (1983).

[11] B. Ramachandran and K. G. Kay, J. Chem. Phys. **83**, 6316 (1985).

[12] M. V. Berry and M. Robnik, J. Phys. A **17**, 2413 (1984).

[13] H.-D. Meyer, E. Haller, H. Koppel, and L. S. Cederbaum, J. Phys. A **17**, L831 (1984); Th. Zimmerman, H.-D. Meyer, H. Koppel, and L. S. Cederbaum, Phys. Rev. A **33**, 4334 (1986).

[14] T. Terasaka and T. Matsushita, Phys. Rev. A **32**, 538 (1985).

[15] M. V. Berry, J. Phys. A **10**, 2083 (1977).

[16] S. W. McDonald and A. N. Kaufman, Phys. Rev. Lett. **42**, 1189 (1979).

[17] R. M. Stratt, N. C. Handy, and W. H. Miller, J. Chem. Phys. **71**, 3311 (1979).

[18] M. Shapiro and G. Goelman, Phys. Rev. Lett. **53**, 1714 (1984).

[19] I. C. Percival, J. Phys. B **6**, 1229 (1973).

[20] A. Voros, in *Stochastic Behavior in Classical and Quantum Systems*, edited by G. Casati and J. Ford (Springer, Berlin, 1979).

[21] M. Feingold, N. Moiseyev, and A. Peres, Chem. Phys. Lett. **117**, 344 (1985); A Peres, Phys. Rev. A **30**, 504 (1984); M. Feingold and A. Peres, *ibid.* **34**, 591 (1986).

[22] K. G. Kay, J. Chem. Phys. **72**, 5955 (1980); S. N. Rai and K. G. Kay, *ibid.* **80**, 4961 (1984).

[23] J. S. Hutchinson and R. B. Wyatt, Phys. Rev. A **23**, 1567 (1981).

[24] M. J. Davis and E. J. Heller, J. Chem. Phys. **80**, 5036 (1984).

[25] Y. Weissman and J. Jortner, Phys. Lett. A **83**, 55 (1981).

[26] K. H. Christoffel and P. Brumer, Phys. Rev. A **33**, 1309 (1986).

[27] N. Pomphrey, J. Phys. B **7**, 1909 (1974).

[28] G. Hose and H. S. Taylor, J. Chem. Phys. **76**, 5356 (1982).

[29] E. B. Stechel and E. J. Heller, Annu. Rev. Phys. Chem. **35**, 563 (1984); E. B. Stechel, J. Chem. Phys. **82**, 364 (1985).

[30] P. Pechukas, J. Phys. Chem. **88**, 4823 (1984).

[31] P. Walters, *An Introduction to Ergodic Theory* (Springer, New York, 1982); V. I. Arnold and A. Avez, *Ergodic Problems in Classical Mechanics* (Benjamin, New York, 1969).

[32] These definitions are simple generalizations of those presented in Ref. 11 for the case of global ergodicity. We wish to point out the following corrections to the definitions of Ref. 11: the upper integration limit in Eqs. (6) and (6′) should be ∞ and the denominator of Eq. (4′) should contain a factor of $\langle A|A\rangle^q$.

[33] F. Vivaldi, G. Casati, and I Guarneri, Phys. Rev. Lett. **51**, 727 (1983); C. F. F. Karney, Physica D **8**, 360 (1983).

[34] N. DeLeon and B. Berne, J. Chem. Phys. **75**, 3495 (1981).

[35] D. Carter and P. Brumer, J. Chem. Phys. **77**, 4208 (1982).

[36] M. J. Davis, Chem. Phys. Lett. **110**, 491 (1984).

[37] R. S. MacKay, J. D. Meiss, and I. C. Percival, Physica D **13**, 55 (1984); D. Bensimon and L. P. Kadanoff, *ibid.* **13**, 82 (1984).

[38] M. J. Davis, J. Chem. Phys. **83**, 1016 (1985) M. J. Davis and S. K. Gray, *ibid.* **84**, 5389 (1986); S. K. Gray, S. A. Rice, and M. J. Davis, J. Phys. Chem. **90**, 3470 (1986).

[39] C. Jaffe and W. P. Reinhardt, J. Chem. Phys. **77**, 5191 (1982).

[40] G. Contopoulos, L. Galgani, and A. Giorgilli, Phys. Rev. A **18**, 1183 (1978). See the remarks on this work appearing in Ref. 1, p. 285.

[41] S. C. Farantos and J. Tennyson, J. Chem. Phys. **84**, 6201 (1986).

[42] H. V. Kuz'min, I. V. Nemov, A. A. Stuchebrukhov, V. N. Bagratashvili, and V. S. Letokhov, Chem. Phys. Lett. **124**, 502 (1986).

[43] E. J. Heller, Faraday Discuss. Chem. Soc. **75**, 141 (1983); E. J. Heller and R. L. Sundberg, in *Chaotic Behavior in Quantum Systems*, edited by G. Casati (Plenum, New York, 1985).

[44] D. W. Noid and R. A. Marcus, J. Chem. Phys. **67**, 559 (1977).

[45] G. Hose and H. S. Taylor, Chem. Phys. **84**, 375 (1984).

[46] I. Hamilton and P. Brumer, J. Chem. Phys. **78**, 2682 (1983).

[47] M. L. Koszykowski, D. W. Noid, M. Tabor, and R. A. Marcus, J. Chem. Phys. **74**, 2530 (1981).

[48] G. Benettin, L. Galgani, and J.-M. Strelcyn, Phys. Rev. A **14**, 2338 (1976).

[49] J. D. Louck and W. H. Shaffer, Mol. Spectrosc. **4**, 285 (1960).

[50] The Hamiltonian diagonalized was similar to that obtained by T. Uzer and R. A. Marcus, J. Chem. Phys. **82**, 4611 (1984), except that a cruder quantization rule was used.

[51] R. T. Skodje, F. Borondo, and W. P. Reinhardt, J. Chem. Phys. **82**, 4611 (1985).

[52] T. P. Grozdanov, S. Saini, and H. S. Taylor, Phys. Rev. A **33**, 55 (1986).

[53] G. Walker and J. Ford, Phys. Rev. **188**, 416 (1969).

[54] This can be inferred, e.g., from the rms energy deviations appearing in Refs. 51 and 52.

[55] R. C. Brown and R. E. Wyatt, Phys. Rev. Lett. **57**, 1 (1986); J. Phys. Chem. **90**, 3590 (1986).

[56] M. J. Davis, E. B. Stechel, and E. J. Heller, Chem. Phys. Lett. **76**, 21 (1980).

[57] G. Hose, H. S. Taylor, and Y. Y. Bai, J. Chem. Phys. **80**, 4363 (1984); K. Stefanski and H. S. Taylor, Phys. Rev. A **31**, 2810 (1985); Y. Y. Bai, G. Hose, K. Stefanski, and H. S. Taylor, *ibid.* **31**, 2821 (1985).

[58] J. Manz and H. H. R. Schor, J. Phys. Chem. **90**, 2030 (1986), and references therein.